Energy Conversion and Management 225 (2020) 113434

Contents lists available at ScienceDirect

Energy Conversion and Management

journal homepage: www.elsevier.com/locate/enconman

Development of a clean power plant integrated with a solar farm for a sustainable community

Shaimaa Seyam *, Ibrahim Dincer, Martin Agelin-Chaab

Faculty of Engineering and Applied Science, Ontario Tech. University, Oshawa, Ontario, Canada

ARTICLE INFO

Keywords:
Solar farm
Hydrogen
Hydrogen liquefaction
Combined cycle
Desalination
Sustainable community
Efficiency

ABSTRACT

Renewable energy sources are attracting attention as a replacement of fossil fuel-based sources. This paper presents a new renewable combined cycle power plant to deliver smart services for a sustainable community. A case study is undertaken for the Kedron Community in the city of Oshawa in Canada. The integrated power plant depends on solar radiation and seawater. The services produced are electric power, heating load, fresh water, and liquified hydrogen as a clean fuel. The combined plant consists of six subsystems: solar farm, Gas turbine cycle, Rankine cycle, multi-effect desalination, electrolyzer, and hydrogen liquefaction subsystem. The integrated system has been studied thermodynamically to investigate the thermal and exergy performance. The solar farm uses HITEC with a mass flow rate of 2000 kg/s to produce an overall heat of 201.3 MW to the combined cycle. The combined cycle delivers 133.1 MW of electric power, a heating load of 284 MW for desalination, and a heating load of 98.2 MW for residential applications. The multistage flash desalination system provides 684 kg/s of fresh water, where 32.09 kg/s is used for electrolysis to produce hydrogen gas. The hydrogen liquefaction system consists of nitrogen precooling refrigeration system, hydrogen Claude refrigeration system, and hydrogen liquefying stream. This liquefaction system produces 355 ton/day of liquefied hydrogen with SFC of 5.24 kWh/kg-LH_2. The overall thermal efficiency of the integrated system is 88.12%, while the exergetic efficiency is 23.05%.

1. Introduction

The increases in population and the growth of urbanization have significant effects on energy consumption. The electricity generation tends to rise slightly every year to fulfill the increasing demand, which is amounted to 1581.7 TWh in 2017 compared to 467 TWh in 1990, representing a 37% increase [1,2]. Fossil fuels such as natural gas, crude oil and coal constitute the major primary energy production of about 60% in total compared to 5% hydro, 29% nuclear, and 3% other renewable sources in 2017 [3]. The GHG emissions from coal-fired electricity generation were recorded as 110 Mt CO_2 eq. in 2000 and dropped to 70 Mt Co_2 eq. in 2017 because of a coal phase-out action plan started in 2001 [3]. These emissions affect the environment, human health and daily activities, resulting in an overall impact on the economy [4].

Numerous researchers have extensively studied the utilization of renewable sources to replace fossil fuels. The superior substitute is the solar energy to replace the thermal energy of power generation because it is carbon neutral and environmentally benign. There are four kinds of thermal solar energy systems: solar power tower, Fresnel reflectors, dish Stirling and parabolic trough to collect and concentrate thermal energy from the sun [5]. The spatial and temporal fluctuation of solar energy is a major challenge its implementation alone. Therefore, the hybridization of solar energy with traditional power plants can be useful to eliminate fossil-burning boilers.

The integration of solar energy with power plants have been studied for different purposes. For examples, Askari and Ameri [6] investigated the integrated linear Fresnel Rankine cycle in Kish island on the southern coast of Iran. The solar Rankine cycle (SRC) comprises two low and high turbines, two pumps, a feedwater heater, two linear Fresnel (LF) solar fields and a condenser, which can be replaced with low temperature multi-effect desalination system. The inlet and outlet HTF temperature to LF was recorded to 295 °C and 397 °C, respectively. This SRC can produce electric power of 137 MW for using a desalination unit and 193 MW for a condenser only. The thermal efficiency is 31% for desalination and 37% for a condenser. Furthermore, Mehrpooya et al. [7] have studied the parabolic trough (PT) collectors with combined systems consisting of the gas turbine cycle and simple organic Rankine cycle (ORC). The heat transfer fluids were selected to be HITEC molten salt in the PT system and refrigerant R113 in the ORC. The overall thermal and exergetic

* Corresponding author.
E-mail addresses: shaimaa.seyam@ontariotechu.net (S. Seyam), Ibrahim.dincer@uoit.ca (I. Dincer), Martin.Agelin-Chaab@uoit.ca (M. Agelin-Chaab).

https://doi.org/10.1016/j.enconman.2020.113434
Received 18 June 2020; Received in revised form 7 September 2020; Accepted 8 September 2020
Available online 30 September 2020

Nomenclature

Symbols

C	Conversion coefficient
$\dot{E}x$	Exergy flow rate, kW
g	Gravitational acceleration, m/s^2
h	Specific enthalpy, kJ/kg
K	Conversion percentage, %
LH_2	Liquefied hydrogen
$\dot{m}$	Mass flow rate, kg/s
n	Number of moles, kmol
Nu	Nusselt number
P	Pressure, kPa
$\dot{Q}$	Heat transfer, kW
R	Gas universal constant,
S	Entropy, kJ/K
s	Specific entropy, kJ/kg.K
T	Temperature, K
V	Velocity, m/s
$\dot{W}$	Power, kW

Greek symbols

μ	Chemical potential,
η	Energetic efficiency
ψ	Exergetic efficiency

Abbreviations

CCPP	Combined-cycle power plant
COP	coefficient of performance
DPB	Discounted payback
GOR	Gained output ratio
GT	Gas turbine cycle
HCRC	Hydrogen Claude refrigeration cycle
HL	Hydrogen liquefaction
HLS	Hydrogen liquefaction stream
IRR	Interest rate of return
LCOE	Levelized cost of energy
MED	Multi-effect desalination
MTA	Minimum temperature approach
NPV	Net present value
PEM	Proton exchange membrane
PI	Profitability index
PRC	Precooling refrigeration cycle
RC	Rankine cycle
ROI	Return of investment
SF	Solar farm
SEC	Specific energy consumption

Subscripts

cd	cold side
ch	chemical
cv	closed volume
des	destruction
ht	hot side
i	inlet
ith	Component *i* in the mixture
in	inflow
o	outlet
out	outflow
overall	overall system
P	products
ph	physical components
R	reactants
s	source
th	thermal

efficiencies are 47% and 38.2%, respectively. The net power produced from this combined power plant is 37.7 MW, while solar power production contributes about 34% of the total power required.

Also, water desalination systems have been considered for investigation with solar energy. For large scale power plants, Askari and Ameri [6] investigated the combination of linear Fresnel solar field with multi effect desalination (MED) system. The MED consists of 14 effects and two gain output ratios (GOR) of 9.8 and 12. Top brine temperature and minimum brine temperature were about 70 and 35 °C, respectively. The temperature drop per effect was about 2.8 °C. The distilled water was obtained to be 100,000 m^3/day, and the specific heat consumption was in the range of 54 to 66 kWh/m^3. The feed seawater temperature was 35 and increased to 66 °C. In addition, Frantz and Seifert [8] investigated the combination of multi-effect desalination with a solar central receiver system and Rankine cycle. The steam temperature varied from 66 °C to 90 °C, the seawater temperature was 35 °C, and the top brine temperature was in the range of 55 to 70 °C. It has resulted that the gain output ratio was in the range of 2.5 to 5.5, and the power consumption of MED was in the range of 1.5 to 2.5 kWh/m^3. Another example, Farsi and Dincer [8] designed a geothermal power plant to produce distilled water, cooling load, power, and hydrogen gas. The desalination system is a combined system of multi-effect desalination (MED) and direct-contact membrane distillation (DCMD). The MED has six effect units, input seawater temperature of 20 °C, top brine temperature of 62 °C. The DCMD has three cells, feed seawater temperature of 47 °C, and total effective membrane area of 325.6 cm^2. The desalination system produced 165 ton/day fresh water. In addition, the GOR for MED can be determined as 5.6, while the mass flux through the hydrophobic permeate was calculated to be 9.8 μm/s.

Furthermore, researchers are interested in large-scale hydrogen production through renewable sources. Berstad et al. [9] developed innovative large-scale hydrogen liquefaction based on mixed-refrigerant pre-cooling system and a reversed helium/neon Brayton cycle. They presented two MR process with Joule Thomson throttling and liquid expanders. The hydrogen feed conditions are 1 kg/s, 300 K, and 21 bar. The specific liquefaction power is in the range of 6.15–6.51 kW/kg-LH_2, and the exergy efficiency of the system is 45–48%. In addition, Aasadnia and Mehrpooya [10] presented a new configuration of for a hydrogen liquefier to produce 90 ton/day. The system comprises of a mixed refrigerant (MR) refrigeration cycle and a cascade Joule-Brayton cycle. The process involves an absorption refrigeration system to cool some hydrogen streams in the precooling and cryogenic sections. The SEC is 6.47 kWh/kg-LH_2, and the exergy efficiency is 45.5%. Moreover, Seyam et al. [11] designed a hybrid system to produce multiple services. The hybrid system consists of PV solar panels, and wind turbines, proton exchange membrane electrolyzer, an absorption cooling system. The services are 0.2 kg/s hydrogen gas, cooling load of 40 and 120 kW, and electric power of 65 and 76.6 kW, for two cases in Egypt and Saudi-Arabia. The overall energetic and exergetic efficiencies are about 67% in all cases. Furthermore, Seyam et al. [12] developed a hydrogen liquefaction system consisting of nitrogen precooling refrigeration cycle and hydrogen Claude refrigeration cycle to produce 335 ton/day. The hydrogen feed conditions are 3.5515 kg/s at 290 K and 200 kPa. The specific energy consumption is 6.41 kWh/kg-LH_2. The energetic and exergetic efficiencies of the liquefaction are 19.8% and 63.4%. The power consumption for the liquefaction and the electrolyzer is 107 MW. Then a design for geothermal and organic Rankine power plant is presented to produce 130 MW to fulfill the power consumption of hydrogen liquefaction and other community services.

Common powerplants are to provide extra services beside the electricity, such as fresh water or clean fuel. Therefore, it is recommended to enlarge the output services from the powerplant to include electricity, clean fuel, and fresh water from renewable resources such as solar energy with thermal storage to maintain the thermal stability over the year. Therefore, this paper presents an innovative, integrated power plant using parabolic trough solar collectors and seawater to provide four services, which are electric power, heating load, freshwater, and liquefied hydrogen. The objectives of this paper are to provide a complete thermodynamic analysis of the integrated system, including evaluation of the energetic and exergetic efficiencies of subsystems and the entire system, and the exergy destruction rates of components, and to conduct parametric studies to investigate the change in parameters on the overall efficiency, such as the change of solar intensity with respect to the tilt angle of solar collector, and the air mass flow, and high pressure of the combined cycle.

2. System description

The power plant consists of five main subsystems: solar farm (SF), combined-cycle powerplant (CCPP), multi-effect desalination (MED), electrolyzer, and hydrogen liquefaction (HL) systems, as shown in Fig. 1. The SF contains solar parabolic cells, hot thermal tank, cold thermal tank, and a boiler heat exchanger (S-HX). The heat transfer fluid (HTF) is selected to be HITEC molten salts.

The CCPP consists of the topper system of regeneration gas turbine (GT) and the bottomed system of Rankine cycle (RC). The air is compressed by the compressor (G-C) then heated before entering the combustion chamber burning with a mixture of fuel. The exhaust gases are expanding through the turbine (G-T). Then, the exhaust gases are used for heating the G-C exit and the superheater heat exchanger (W-HX). The bottomer system of (RC) is pressurizing the circulating freon fluid by a pump. The freon is heated by S-HX heat exchanger for vapour phase and then by W-HX heat exchanger for the superheated phase. Then the steam is expanded by the turbine of W-T to generate the power. After the expansion, the freon steam is condensed through W-EV by recirculating water, which is used for MED system.

The MED system uses seawater to produce fresh water through three desalination units. The seawater is heated through a heat exchanger (D18) enters the three units through sprays. The first unit uses the heat from the condenser of CCPP to heat the seawater to the liquid–vapour phase. The pure vapour with no salt exits the unit from the side, while the liquid phase with high salinity exits the unit from the bottom. The pure unsalted vapour is used to heat the other desalination unit to repeat the same process by separating the unsalted vapour and salted liquid. All the brine fluid is collected to the brine reject. Also, all unsalted vapour is condensed and cooled to be fresh water.

Some of the electricity generated is used for electrolyzer to chemically split water into oxygen gas and hydrogen gas. The hydrogen gas is used for the HL process for clean transportation. Another part of the electricity generated is used for the HL process. This process consists of three main subsystems: the hydrogen Claude refrigeration cycle (HCRC), precooling refrigeration cycle (PRC), and hydrogen liquefaction stream (HLS). The HCRC consists of two compressors with two condensers, nine heat exchangers, three turbines, and a separator. The two compressors divide the pressure of the cycle into three paths: high-pressure path (HPP), medium-pressure path (MPP), and low-pressure path (LPP). The PRC consists of four compressors with four condensers, an expander, a separator, and two heat exchangers. The PRC is used to cool the HPP through two exchangers R-HX1 and R-HX2. The eight heat exchangers are used to cryogenically cool the hydrogen gas of HLS though a catalyst (the iron (III) hydroxide ($Fe(OH)_3$)) [13]. This catalyst chemically separates the hydrogen into para-hydrogen and ortho-hydrogen. The more the content of para-hydrogen, the more stable hydrogen is to stay in the liquid phase [14].

3. Case study

The community of study is the Kedron Planning area, which is located in the city of Oshawa between Conlin Rd East and Road 407 [15], as shown in Fig. 2. Based on the report of community profile in 2017, the Kedron planning is 85% under-developed, with a planned capacity of 22,000 new residents over 1,151 acres of land, which is about 3% of the City of Oshawa [15]. This plan includes 7 new schools, several parks and nearly 4000 homes and dwellings [16]. The water consumption was found to be 220 L of water per person per day [17] for residential water in 2017. In addition, energy consumption is estimated to be 101 GJ per household (28,056 kWh/household) in the province of Ontario in 2017 [18]. That includes the electrical consumption for a household of an average of 11,879 kWh/year [19,20], and the heating load per household of 14 kW [21]. Furthermore, the annual energy consumption per unit area by the school is approximately 67–240 [kWh/m^2/yr], which varies considerably between schools [22]. Assuming that the new schools have a floor area of 3600 m^2 and cooling/heating area of 3173 m^2. This energy consumption will include thermal energy consumption due to the heating of 150 kWh/m^2 and electrical energy consumption of 100 kWh/m^2 [23]. Therefore, the combined power plant for this community includes a solar farm, combined-cycle power plant, multi-effect desalination, electrolyzer, and liquefaction systems, as explained in Fig. 2. The main sources are clean, sustainable energy sources such as the sun and ocean.

Based on the given information in the previous paragraph, the total water consumption, heating load, and electric energy consumption for the selected community are estimated to be 66 kg/s, 58,870 kW, and 8,275 kW, respectively. Based on the literature, the hydrogen liquefaction power and electrolyzer power are estimated to about 80 MW and 20 MW [12], respectively. Therefore, the total power generated from the combined cycle power plant should provide three major power requirements: hydrogen liquefaction of 80,000 kW, electrolyzer of 20,000 kW, and community services of about 10,000 kW, which is more than the community requirements for extra services in future such as expansion, industry, and health services. Therefore, the total power of the combined powerplant will be evaluated to be 110,000 kW (110 MW).

4. System analysis

In this section, the general balance equations are described for the entire system. Also, the governing equations for the solar farm, multi-effect distillation system and hydrogen liquefaction systems. Some assumptions are considered in the thermodynamic analysis as follows:

- No pressure drops in pipes and heat exchangers.
- No heat losses in pipes, turbines, compressors, condensers, heat exchangers, and flash separators.
- The turbines and compressors have thermal isentropic efficiencies of 80% and 85% and optimal mechanical efficiencies.
- The kinetic and potential energies are neglected since the changes in velocities and elevation across the system are small compared to flow energy, work, and heat.
- All processes are performed under steady state conditions.

Thermodynamic modeling was performed using the Aspen Plus and Engineering Equation Solver (EES) software packages, which produce accurate results and includes a large library of substances. The EES was used for solar farm and electrolyzer systems, while the remaining systems were modeled by Aspen Plus. Two equation of states (EOS) are chosen: Peng-Robinson model for CCPP and HL systems [25–27], and ELECNTRL for MED system [28,29] since it is convenient for modeling salts.

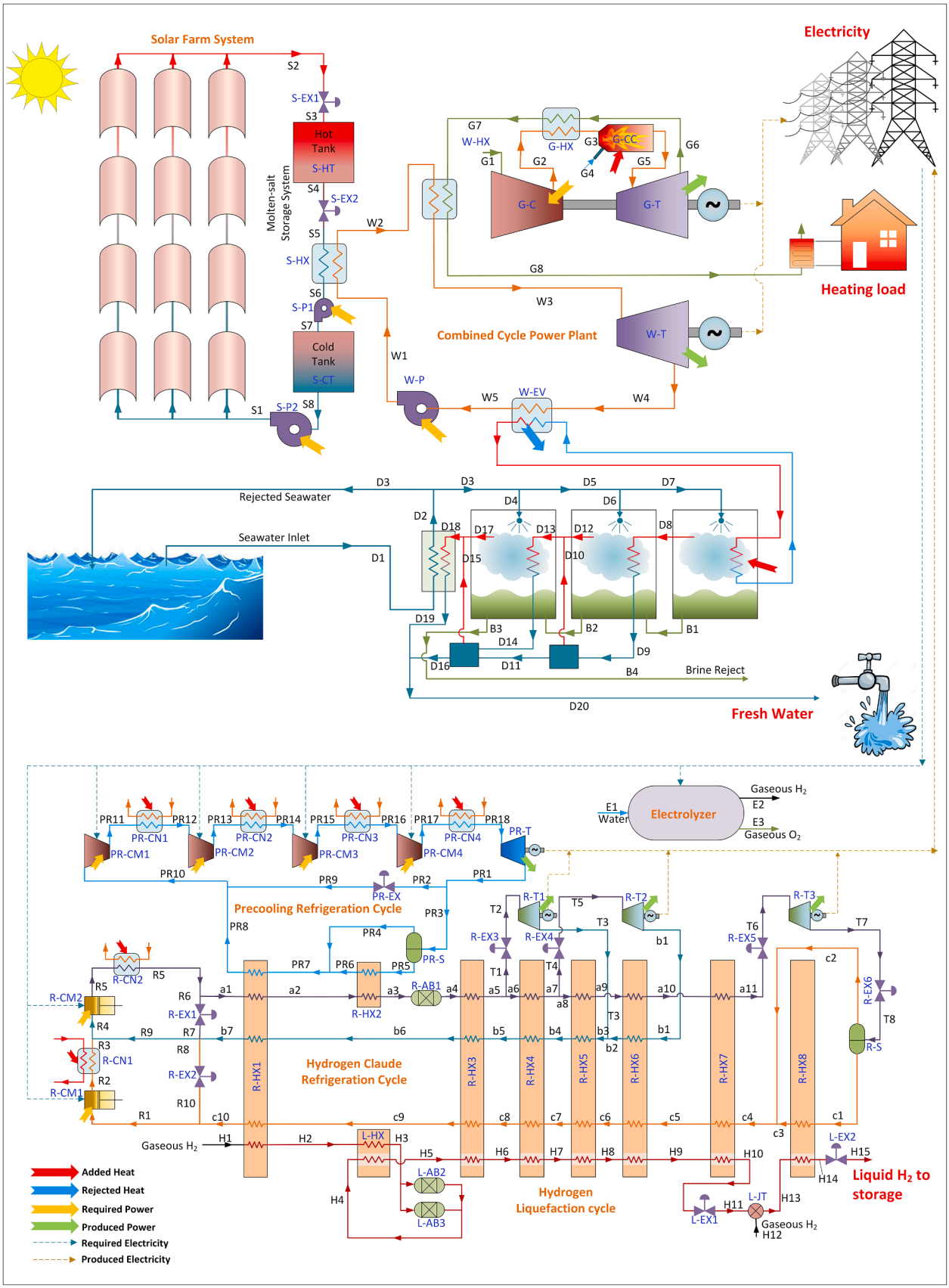

Fig. 1. Schematic diagram of the present integrated system.

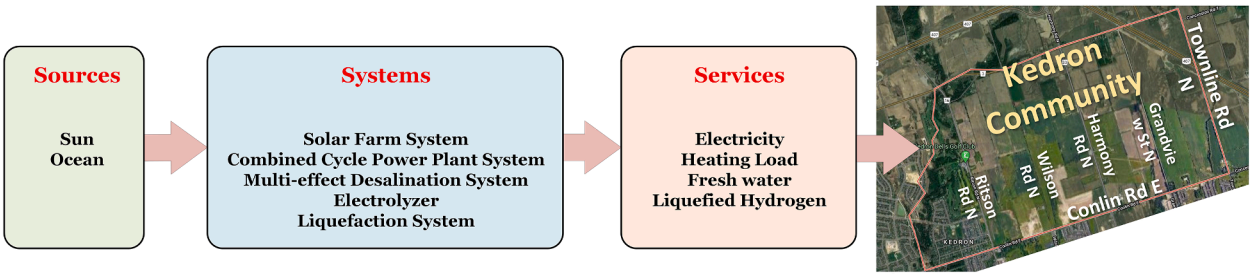

Fig. 2. The layout of combined power plant for the Kedron Planning in the city of Oshawa (adapted from Google Map [24]).

4.1. Balance equations

Three balance equations are studies for each component: mass, energy, and exergy balance equations. The mass balance equation for a steady state flow process is expressed in a general form as Eq. (1).

$$\sum \dot{m}_{in} = \sum \dot{m}_{out} \tag{1}$$

The energy balance equation for steady flow process can be generalized to be as

$$\dot{Q}_{cv} - \dot{W}_{cv} + \sum \dot{m}_i \left(h_i + \frac{1}{2}V_i^2 + gz_i \right) - \sum \dot{m}_o \left(h_o + \frac{1}{2}V_o^2 + gz_o \right) = 0 \tag{2}$$

where $\dot{Q}_{cv}$ and $\dot{W}_{cv}$ represents the heat transfer and the work crossing the boundaries of the system. The steady energy flow is expressed as $(h + 0.5V^2 + gz)$, which represents kinetic energy, and the specific enthalpy, V is the stream velocity of the working fluid, g is the gravitational acceleration, and z is the elevation from a reference point. Also, the exergy balance equation for a steady flow process can be expressed as

$$\sum \dot{m}_{in} ex_{in} = \sum \dot{E}x_{th} + \sum \dot{E}x_{w} + \sum \dot{m}_{out} ex_{out} + \dot{E}x_{des} \tag{3}$$

where $\dot{E}x_{th}$ denotes the thermal exergy with the heat energy exchange across the system volume and is expressed as $\dot{E}x_{th} = (1 - T_o/T_s)\dot{Q}$. $\dot{E}x_w$ denotes the rate of exergy transfer by the boundary or work applied on or done by the system $\dot{E}x_w = \dot{W}$. The total specific exergy of each stream is comprised of physical $ex_{ph,i}$ and chemical exergy $ex_{ch,i}$ and can be described as the following:

$$ex_i = ex_{ph,i} + ex_{ch,i} \tag{4}$$

$$ex_{ph,i} = (h_i - h_o) - T_o(s_i - s_o) \text{ and } ex_{ch,i} = \sum n_i(\mu_i^o - \mu_i^\infty) \tag{5}$$

where s is the specific entropy, subscript o stands for the dead state, T_o is the ambient temperature, μ_i^o is the chemical potential of ith component in thermomechanical equilibrium, and μ_i^∞ is chemical potential of ith component in chemical equilibrium. In addition, the specific exergy $\dot{E}x_{ch} = \dot{m}ex_{mix}^{ch}$ of the gas mixture can be expressed as equation (6), where x_i is defined as the molar fraction of gas i in the gas mixture.

$$ex_{mix}^{ch} = \left[\sum_{i=1}^{n} x_i ex^{c,i} + RT_o \sum_{i=1}^{n} x_i ln x_i \right] \tag{6}$$

The proposed systems consist of turbines, compressors, pumps, flash separators, heat exchangers, condensers, and expansion valves. Therefore, the mass, energy, exergy balance equations are expressed in a general form and listed in Table 1.

4.2. Solar farm system

The solar farm contains parabolic trough collectors (PTC), which consists of a receiver tube and a collector mirror. The HTF is HITEC molten-salt flowing through the receiver tubes and the rest of the system. The HITEC molten-salt is a ternary mixture of alkali-nitrates/nitrites used for thermal storage material in solar systems. The specifications of HITEC molten-salt are tabulated in Table 2, which are functions of the fluid bulk temperature in Kelvin.

The collector reflects and concentrates the sun rays to the receiver to heat the HTF. The amount of flux absorbed by the receiver tube is given by [7]

$$S = I_b R_b (\tau\alpha)_b \rho\gamma + I_b R_b (\tau\alpha)_b \left(\frac{D_o}{W - D_o} \right) \tag{7}$$

where S is beam radiation [W/m^2], I_b is the incident solar intensity [W/m^2], ρ is the mirror reflectivity, τ is transmissivity of glass, α is absorptivity of a mirror, $(\tau\alpha)_b$ is the transmittance-absorptance product, γ is considered to be fixed as equivalent to 0.95, D_o is the receiver outside tube diameter, and W is the aperture width of PTC collector. Moreover,

Table 1
Mass, energy, exergy balance equations for basic components in the integrated system.

Components	Mass balance	Energy balance	Exergy balance
Compressors	$\dot{m}_{in,c} = \dot{m}_{out,c}$	$\dot{W}_c = \dot{m}_c(h_{out,c} - h_{in,c})/\eta_c$	$\dot{m}_{in,c}ex_{in,c} + \dot{W}_c = \dot{m}_{out,c}ex_{out,c} + \dot{E}x_{des,c}$
Turbines	$\dot{m}_{in,t} = \dot{m}_{out,t}$	$\dot{W}_t = \eta_t\dot{m}_t(h_{in,t} - h_{out,t})$	$\dot{m}_{in,t}ex_{in,t} = \dot{W}_t + \dot{m}_{out,t}ex_{out,t} + \dot{E}x_{des,t}$
Pumps	$\dot{m}_{in,p} = \dot{m}_{out,p}$	$\dot{W}_p = \dot{m}_p(h_{out,p} - h_{in,p})/\eta_p$	$\dot{m}_{in,p}ex_{in,p} + \dot{W}_p = \dot{m}_{out,p}ex_{out,p} + \dot{E}x_{des,p}$
Condensers	$\dot{m}_{in,cn} = \dot{m}_{out,cn}$	$\dot{Q}_{cn} = \dot{m}_{cn}(h_{out,cn} - h_{in,cn})$	$\dot{m}_{in,cn}ex_{in,cn} = (1 - T_o/T_s)\dot{Q}_{cn}^{\text{Å}} + \dot{m}_{out,cn}ex_{out,cn} + \dot{E}x_{des,cn}$
Heat exchangers	$\sum_i \dot{m}_{in,cd} = \sum_i \dot{m}_{out,cd}$ $\sum_i \dot{m}_{in,ht} = \sum_i \dot{m}_{out,ht}$	$\dot{Q}_{ht} = \sum_i \dot{m}_{ht}(h_{out,ht} - h_{in,ht})$ $\dot{Q}_{cd} = \sum_i \dot{m}_{cd}(h_{in,cd} - h_{out,cd})$ $\dot{Q}_{cd} = \dot{Q}_{ht}$	$\sum_i \dot{m}_{ht}ex_{in,ht} + \sum_i \dot{m}_{cd}ex_{in,cd} = \sum_i \dot{m}_{ht}ex_{out,ht} + \sum_i \dot{m}_{cd}ex_{out,cd} + \dot{E}x_{des,hx}$
Expansion valves	$\dot{m}_{in,ex} = \dot{m}_{out,ex}$	$h_{in,ex} = h_{out,ex}$	$\dot{m}_{in,ex}ex_{in,ex} = \dot{m}_{out,ex}ex_{out,ex} + \dot{E}x_{des,ex}$
Flash separators	$\dot{m}_{in,f} = \sum \dot{m}_{out,f}$	$\dot{m}_{in,f}h_{in,f} = \dot{m}_{out,f,v}h_{out,f,v} + \dot{m}_{out,f,l}h_{out,f,l}$	$\dot{m}_{in,f}ex_{in,f} = \dot{m}_{out,f,v}ex_{out,f,v} + \dot{m}_{out,f,l}ex_{out,f,l} + \dot{E}x_{des,f}$
Reactors	$\sum_R \dot{m}_{in,R} = \sum_P \dot{m}_{out,P}$	$\sum_R \dot{m}_{in,R}h_{in,R} = \dot{Q}_{out,r} + \sum_P \dot{m}_{out,P}h_{out,P}$	$\sum_R \dot{m}_{in,R}ex_{in,R} = (To/Ts, r - 1)\dot{Q}_{out,r} + \sum_P \dot{m}_{out,P}ex_{out,P} + \dot{E}x_{des,r}$
Electrolyzer	$\dot{m}_w = \dot{m}_{O_2} + \dot{m}_{H_2}$	$\dot{W}_e + \dot{m}_{w,R}h_{w,R} = \dot{m}_{O_2}h_{O_2} + \dot{m}_{H_2}h_{H_2}$	$\dot{W}_e + \dot{m}_{w,R}ex_{w,R} = \dot{m}_{O_2}ex_{O_2} + \dot{m}_{H_2}ex_{H_2} + \dot{E}x_{des,e}$

Table 2
The properties of HITEC [30].

Property	Value
HITEC components (wt%)	7% $NANO_3$ + 40% $NANO_2$ + 53% KNO_3
Density [kg/m^3]	1640 at 300 °C $\rho = -0.733(T-273.15) + 2080$
Dynamic viscosity [Pa.s]	0.00316 at 300℃ $b = \frac{5.9(T-9.638)}{990.362}$ and $\mu = \frac{e^{b}+e^{-b}}{e^{b}-e^{-b}} - 0.999$
Specific heat capacity [kJ/kg.K]	1.56 at 300 °C $C_P = 1.560 - (T-273.15)/1000$
Thermal conductivity [W/m.K]	0.2 at 300 °C $k = 0.78 - 1.25\times10^{-3}T + 1.6\times10^{-6}T^2$
Melting point [℃]	142
Maximum working temperature [℃]	355
HITEC mass flow rate [kg/s]	2000

R_b is described as Eq. (8).

$$R_b = \frac{\cos\theta}{\sin\psi\sin\delta + \cos\psi\cos\delta\cos\lambda} \tag{8}$$

where ψ is Latitude, for the city of Oshawa which is (43.8971° N, 78.8658° W), λ is hour angle [°], θ is incident angle [°], β is tilt angle, γ is wall azimuth angle due to south direction, and δ is declination angle throughout the year.

The amount of useful heat transferred to the HTF, which is flowing within the receiver tube based on the absorbed radiation concept, can be calculated using

$$\dot{Q}_u = F_R[SA_a - A_r U_L(T_i - T_a)] \tag{9}$$

The fluid exit temperature can be computed by:

$$T_o = T_i + \frac{\dot{Q}_u}{\dot{m}C} \tag{10}$$

To obtain the amount of useful energy absorbed by the HTF, the temperature of the glass cover was first guessed. Then the heat loss coefficient was calculated by $Nu = 0.023\times Re^{0.8}\times Pr^{0.4}$, since the Reynolds number is $Re = \rho V D_i/\mu$ and the flow is turbulent if Re is greater than 2300. For laminar flow (Re < 2300), the Nusselt number is constant and equal to 4.364.

Finally, the actual temperature for the glass cover is achieved by iteration. The collector heat removal factor was achieved using the following equation:

$$F_R = \frac{\dot{m}C}{A_r U_L}\left[1 - \exp\left(\frac{-A_r U_L F^{'}}{\dot{m}C_P}\right)\right] \tag{11}$$

where $\dot{m}$ is HTF mass flow rate [kg/s], C_P is the specific heat of HITEC [J/kg.K], A_r is receiver tube area, and F' refers to the collector efficiency factor and could be computed according to the following equation.

$$F^{'} = \frac{\frac{1}{U_L}}{\frac{1}{U_L} + \frac{D_o}{h_{fi}D_i} + \left[\frac{D_o}{2K}\ln\left(\frac{D_o}{D_i}\right)\right]} \tag{12}$$

where D_i and D_o are the inner and outer diameter of receiver tube, respectively. h_{fi} is the convective heat transfer coefficient with the tube and can be calculated from the standard pipe flow equation $h_{fi} = Nu\times K/D_i$ and $Nu = 0.023\times Re^{0.8}\times Pr^{0.4}$. The convection heat transfer between the receiver tube and the glass cover is neglected because the space between them is evacuated. Therefore, the overall heat loss coefficient considering the convection, radiation, and conduction losses according to the receiver tube area is given as follows:

$$U_L = \left[\frac{A_r}{(h_w + h_{r,g-a})A_g} + \frac{1}{h_{r,g-a}}\right]^{-1} \tag{13}$$

where $h_{c,g-a}$ is the glass cover convective heat transfer coefficient is calculated as $h_{c,g-a} = h_w = Nu.K/D_g$, where Nu is calculated as $Nu = 0.3\times Re^{0.6}$ for [1000 < Re < 50,000], $h_{r,g-a}$ is the glass cover radiation heat transfer coefficient and evaluated as $h_{r,g-a} = \varepsilon_g\sigma(T_g + T_a)\left(T_g^2 + T_a^2\right)$

In addition, the radiation heat transfer coefficient between the receiver tube and glass cover is estimated by:

$$h_{r,r-g} = \frac{\sigma(T_r + T_g)\left(T_r^2 + T_g^2\right)}{\frac{1}{\varepsilon_r} + \frac{A_r}{A_g}\left(\frac{1}{\varepsilon_g} - 1\right)} \tag{14}$$

Since the value obtained for the overall heat loss coefficient is based on the assumed value for the glass cover temperature. Therefore, the correction of the assumption considered should be checked. Thus, the glass cover actual temperature is calculated by

$$T_g = \frac{A_r h_{r,r-g}T_r + A_g(h_w + h_{r,g-a})T_a}{A_r h_{r,r-g} + A_g(h_w + h_{r,g-a})} \tag{15}$$

where A_r is receiver tube area, A_g is glass cover area, A_a is unshaded collector aperture area. The specifications of solar panels used in this study are given in Table 3, which combined the receiver properties, the collector structure, and mirror optical properties. The thermal efficiency of solar PTC, η_{PTC}, and the SF system, η_{SF}, are given as:

$$\eta_{PTC} = \frac{\dot{Q}_u}{SA_a} \text{ and } \eta_{SF} = \frac{\dot{m}_S C_S(T_{S5} - T_{S6})}{SA_a} \tag{16}$$

The exergy efficiency of a solar farm is determined to be as the following:

$$\psi_{PTC} = \frac{\dot{E}x_u^{Q}}{\left[1 - \frac{4}{3}\left(\frac{T_o}{T_{sun}}\right) + \frac{1}{3}\left(\frac{T_o}{T_{sun}}\right)^4\right]SA_a} \text{ and}$$
$$\psi_{SF} = \frac{\dot{E}x_{S5} - \dot{E}x_{S6}}{\left[1 - \frac{4}{3}\left(\frac{T_o}{T_{sun}}\right) + \frac{1}{3}\left(\frac{T_o}{T_{sun}}\right)^4\right]SA_a} \tag{17}$$

4.3. Combined power system

The CCPC consists of the topper system of GT and the bottomer system of RC. The total power of the CCPC can be expressed as:

$$\dot{W}_{net} = \dot{W}_{G-T} + \dot{W}_{W-T} - \dot{W}_{G-C} - \dot{W}_{W-P} \tag{18}$$

The heating value for houses can be obtained by the heat of exhaust gases multiplied by the efficiency of the furnaces, η_h, which is assumed to be 60%.

$$\dot{Q}_h = \eta_h \dot{m}_{ex}(h_{G8} - h_{G9}) \tag{19}$$

The condenser, W-EV, is used for heating the seawater desalination system. The removed heat is calculated as the following:

$$\dot{Q}_D = \dot{m}_{w4}(h_{W4} - h_{W5}) \tag{20}$$

The thermal efficiency of CCPP is estimated to be:

$$\eta_{CCPP} = \frac{\dot{W}_{net} + \dot{Q}_h + \dot{Q}_D}{\dot{Q}_{G-CC} + \dot{Q}_{S-HX}} \tag{21}$$

The exergy efficiency of CCPP is given as below:

Table 3
The specifications of solar panels.

Specifications	Value
Collector model	ET150 [31]
Receiver model	SOLEL UVAC [32]
Receiver properties	
Outer diameter of absorber, $D_{a,o}$ [m]	0.07
Inner diameter of absorber tube, $D_{a,i}$ [m]	0.065
Outer diameter of glass envelope, $D_{g,o}$ [m]	0.115
Inner diameter of glass envelope, $D_{g,I}$ [m]	0.129
Glass emissivity, ε_g	0.9
Collector structure	
Length of each module, L [m]	12.27
Mirror length in each module [m]	11.9
Focal length [m]	1.71
Effective mirror width [m]	5.552
Aperture width, W [m]	5.77
Effective aperture area [m^2]	817.5
Length of collector assembly [m]	150
Collector row spacing [m]	15
Number of loops	300
Number of modules per collector, n_c	100
Mirror optical properties	
Intercept factor	0.92
Mirror reflectivity, ρ	0.94
Transmissivity of glass, τ	0.945
Solar absorptivity, σ	0.94
Peak optical efficiency	0.768

$$\psi_{CCPP} = \frac{\dot{W}_{net} + \dot{E}x_h^Q + \dot{E}x_D^Q}{\dot{E}x_{G-CC}^Q + \dot{E}x_{S-HX}^Q} \tag{22}$$

The fuel mixture was selected based on real blending ratios from the Air Liquide company, similar to Mixture G-8 [33]. The fuel mixture contains by weight 79.77% methane, 9.40% ethane, 9.12% propane, 0.76% isobutane, 0.57% isopentane, and 0.38% carbon dioxide. The molecular weight of the fuel mixture is 20.66 g/mol and specific density is 45.66 m^3/kg, while the low and high heating values are 48.3 and 52.9 MJ/kg, respectively. In addition, the flowing fluid of RC is chosen to be R245fa (1,1,1,3,3-Pentafluoropropane $C_3F_5H_3$) of 134.03 g/mol molecular weight. Its characteristics are 15.18 °C boiling point, 1338.54 kg/m^3 liquid density, 8.55 kg/m^3 vapour density, and 114.32 kJ/kg latent heat. This freon has a zero ozone depletion potential and 1030 global warming potential [34]. The stoichiometric reactions for each component in the combustion chamber are listed below.

- Methane $CH_4 + 2O_2 \rightarrow CO_2 + 2H_2O$ $\Delta H_c = -891$ kJ/mol
- Ethane $2C_2H_6 + 7O_2 \rightarrow 4CO_2 + 6H_2O$ $\Delta H_c = -1561$ kJ/mol
- Propane $C_3H_8 + 5O_2 \rightarrow 3CO_2 + 4H_2O$ $\Delta H_c = -2220$ kJ/mol
- Isobutane $2C_4H_{10} + 13O_2 \rightarrow 8CO_2 + 10H_2O$ $\Delta H_c = -2871$kJ/mol
- Isopentane $C_5H_{12} + 8O_2 \rightarrow 5CO_2 + 6H_2O$ $\Delta H_c = -3506$ kJ/mol

4.4. Desalination system

The desalination system consists of three effects/units having the same temperature difference. The brine temperature, T_i, is decreased for the next effect by the temperature difference

$$\Delta T = \frac{T_1 - T_n}{n-1} \tag{23}$$

The condensation temperature, T_{vi}, of the vapour generated inside effect i is the difference between the brine temperature, T_i, and the boiling point elevation (BPE).

The feed seawater flow rate, $\dot{m}_{F1}$, is equally distributed to all effects. A constant salinity x_i is assumed throughout all effects. The brine leaving effect i, $\dot{m}_{Bi}$, is introduced into effect $i+1$. Therefore, pure water, $\dot{m}_{Di}$, is leaving the effect and used to heat the next effect. This is repeated until the last effect with no salinity. The mass flow rate of desalinated water is estimated by the following.

$$\dot{m}_{Di} = \sum_{k=1}^{i} \dot{m}_{Fi} - \dot{m}_{Bi} \tag{24}$$

The thermodynamic analysis of the first effect the mass balance, partial mass balance and the energy balance equations, as shown below

$$\begin{aligned} \text{Effect 1} \quad & \dot{m}_{D,1} = \dot{m}_{F,1} - \dot{m}_{B,1} \\ & x_F\dot{m}_F = x_B\dot{m}_B = x_B\left(\dot{m}_F - \dot{m}_D\right) \\ & \dot{Q}_{s,1} = \dot{Q}_{W-EV} = \dot{m}_s c\left(T_{s,in} - T_{s,ex}\right) \\ & \dot{Q}_{s,1} = \dot{m}_{D,1}h_{fg,1} + \dot{m}_{F,1}c(T_1 - T_F) \end{aligned} \tag{25}$$

The desalinated water is used to heat the next effect, and the brine of the previous effect enters the next one and heats the seawater to remove the salinity. The mass balance and the energy balance equations are listed in

$$\begin{aligned} \text{Effect } i \quad & \dot{m}_{D,i} = \dot{m}_{F,i} - \left(\dot{m}_{B,i} - \dot{m}_{B,i-1}\right) \\ & x_F\dot{m}_F + x_{B,i-1}\dot{m}_{B,i-1} = x_{B,i}\dot{m}_{B,i} \\ & \dot{Q}_{s,i} = \dot{m}_{D,i-1}h_{fg,i-1} + \dot{m}_{B,i-1}c(T_{i-1} - T_i) \\ & \dot{Q}_{s,i} = \dot{m}_{D,i}h_{fg,i} + \dot{m}_{F,i}c(T_i - T_F) \end{aligned} \tag{26}$$

The energetic efficiency of the MED can be obtained as the following:

$$\eta_{MED} = \frac{\dot{m}_{D,20}h_{20}}{\dot{Q}_{W-EV}} \tag{27}$$

Other energetic performance can be considered as the gained output ratio (GOR), which is defined as the ratio of the mass flowrate desalinated water from the entire system to the mass flow rate of steam of the condenser.

$$GOR = \frac{\dot{m}_D}{\dot{m}_s} \tag{28}$$

The heat exchanger in the MED, which is located beside the last effect, is used for cooling the desalinated water to be liquid and heating the seawater. This will increase the seawater temperature at the inlet of each effect.

The exergy efficiency of the MED can be described as the following:

$$\psi_{MED} = \frac{\dot{m}_{D,20}ex_{20}}{\left(1 - \frac{T_o}{T_s}\right)\dot{Q}_{W-EV}} \tag{29}$$

4.5. Electrolyzer

A proton exchange membrane (PEM) electrolysis is used for hydrogen production via electrochemical conversion of water to hydrogen and oxygen. The PEM electrolyzer consists of two electrodes and an electrolyte [35,36]. Water is fed to the anode at 290 K and 2 bar, where it is split into oxygen and H^+. Then, the produced proton is transferred through the membrane to the cathode, where it receives electron and forms hydrogen. The reaction regarding the hydrogen production in the PEM electrolyzer can be written as

$$\text{Overall reaction}: \quad 2H_2O + \Delta H \rightarrow 2H_2 + O_2 \tag{30}$$

$$\text{Anodic reaction (oxidation)}: \quad 2H_2O \rightarrow O_2 + 4H^+ + 4e^- \tag{31}$$

$$\text{Cathodic reaction (reduction)}: \quad 2H^+ + 2e^- \rightarrow H_2 \tag{32}$$

The total energy needed for the electrolyzer can be obtained as

$$\dot{W}_e = \Delta G = \Delta H - T\Delta S \tag{33}$$

where ΔG is Gibb's free energy, which is the electrical energy demand to operate the electrolyzer, ΔH is the theoretical energy required for water electrolysis without any loss, and $T\Delta S$ represents the thermal energy requirement. The energy efficiency (η_e) and exergy efficiency of the

electrolyzer (ψ_e) can be written as

$$\eta_e = \frac{\dot{m}_{H_2} h_{H_2}}{\dot{W}_e + \dot{m}_{E1} h_{E1}} \text{ and } \psi_e = \frac{\dot{m}_{H_2} ex_{H_2}}{\dot{W}_e + \dot{m}_{E1} ex_{E1}} \tag{34}$$

4.6. Hydrogen liquefaction

The hydrogen liquefaction system consists of two cycle and one liquified stream. The total required power of the system can be estimated as the total compressor power subtracting the total turbine power that is included in the entire HL system, as shown in

$$\dot{W}_{net} = \sum \dot{W}_{CM,i} - \sum \dot{W}_{T,i} \tag{35}$$

At the ambient temperature, the gaseous hydrogen contains 75% ortho-hydrogen and 25% para-hydrogen [37]. By decreasing the temperature to 20 K, the amount of para-hydrogen is increased to 99.8% while the amount of ortho-hydrogen is decreased to 0.2%. The existence of para-hydrogen in the liquid state stabilizes the liquid phase for a long period, while the liquefactions of gaseous hydrogen at such low temperatures will evaporate within 24 h [38,39]. The path of Hs in Fig. 1 is where the hydrogen liquefied chemically by a catalyst in the heat exchangers of (R-HX3 to R-HX8 and L-HX). The ortho–para hydrogen chemical conversion can be given as:

$$(\text{ortho} - H_2) \rightleftarrows (\text{para} - H_2) + \text{Heat} \tag{36}$$

The properties of ortho-hydrogen are not implemented in Aspen Plus. Therefore, the conversion of normal hydrogen to para-hydrogen is considered since normal hydrogen contains ortho and para-hydrogen, and the main reason for conversion reactors is to convert a certain amount of normal hydrogen into para-hydrogen. Therefore, the chemical conversion can be written as:

$$X_n(\text{normal-}H_2) \rightleftarrows (1 - X_p)(\text{normal-}H_2) + X_p(\text{para-}H_2) + \text{Heat} \tag{37}$$

where X_n and X_p is the mass fraction of normal and para-hydrogen, respectively. That means the total mass fraction of para-hydrogen is estimated as $Y_p = 0.25 + 0.75X_p$ while the total mass fraction of ortho-hydrogen is calculated as $Y_o = 0.75 - 0.75X_p$.

The Aspen Plus was selected for simulation of the entire process. However, it cannot simulate the heat exchanger with a catalyst. Therefore, eight conversion reactors are used to replace the catalyst inside the heat exchanger for the hydrogen liquefaction stream, and they are placed at the heat exchanger downstream of the liquefying path. The conversion stages are considered to be patch-continuous after each heat exchanger. The conversion percentage (K) depends on the hydrogen exit temperature from the heat exchanger as [40,41]:

$$K = C_0 + C_1 T + C_2 T^2 \tag{38}$$

where K is conversion percentage, and T is hydrogen temperature in Kelvin. C_0, C_1, and C_2 are conversion coefficients, which are adjusted to match para-hydrogen percentage of the reactor at a certain temperature T and must equal the experimental data [37].

The energy efficiency of the hydrogen liquefaction system can be expressed as Eq. (33). The figure of merit (FOM) is defined as the ratio of minimum power to the actual net power consumption of the whole process, which is expressed exactly as the exergy efficiency, as shown below.

$$\eta_{HL} = \frac{\dot{m}_{LH_2}(h_{H1} - h_{H15})}{\sum \dot{W}_{CM} - \sum \dot{W}_T} \tag{39}$$

$$\psi_{HL} = \frac{\dot{m}_{LH_2}(ex_{H1} - ex_{H15})}{\sum \dot{W}_{CM} - \sum \dot{W}_T} = FOM \tag{40}$$

The specific energy consumption (SEC) is defined as the ratio of the net power required to liquefy the hydrogen with respect to the amount of liquefied hydrogen as

$$SEC = \frac{\sum \dot{W}_{CM} - \sum \dot{W}_T}{\dot{m}_{LH_2} \times 3600} \tag{41}$$

The minimum theoretical specific liquefaction power (SEC_{min}) is calculated as the difference in exergy rate between the feed and product divided by the mass flow rate of the liquefied hydrogen. Therefore, the SEC_{min} equals to 4.06 kWh/kg_{LH_2}.

$$SEC_{min} = \frac{\dot{E}x_{feed} - \dot{E}x_{product}}{\dot{m}_{LH_2} \times 3600} \tag{42}$$

Thus, the exergy efficiency also can be defined as the ratio of ideal SEC to the actual SEC and can be written as $\psi_{HL} = \frac{SEC_{min}}{SEC}$. The energetic and exergetic COP of nitrogen precooling cycle and hydrogen Claude refrigeration cycles can be estimated as

$$COP_{en,\text{PR}} = \frac{\dot{Q}_{R-HX1} + \dot{Q}_{R-HX2}}{\sum \dot{W}_{CM} - \dot{W}_T} \text{ and}$$
$$COP_{ex,\text{PR}} = \frac{\sum_{i=1}^{2} (T_o/T_{s,i} - 1)\dot{Q}_{R-HXi}}{\sum \dot{W}_{CM} - \dot{W}_T} \tag{43}$$

$$COP_{en,\text{R}} = \frac{\sum_{i=3}^{8} \dot{Q}_{R-HXi}}{\sum \dot{W}_{CM} - \sum \dot{W}_T} \text{ and}$$
$$COP_{ex,\text{R}} = \frac{\sum_{i=3}^{8} (T_o/T_{s,i} - 1)\dot{Q}_{R-HXi}}{\sum \dot{W}_{CM} - \sum \dot{W}_T} \tag{44}$$

where Q_{R-HXi} is the heat transfer to the cold streams which is equal to the heat transfer from the hot stream of the heat exchangers.

5. Results and discussion

This section covers the results of the thermodynamic analysis of each cycle and discusses the performance of systems, which are presented in the following subsections. The Aspen plus flow charts for CCPP, MED, and HL subsystems are illustrated in Fig. 3 (a) to (c).

5.1. Analysis results

Some setting and design assumptions are listed for the entire system, as shown in Table 4. These settings include the ambient conditions, the mass flow rates, and pressure levels of cycles, the feed conditions, and the adiabatic efficiencies of turbomachinery components.

The solar farm produced heat of 201.3 MW to the CCP through the heat exchanger S-HX. This amount of heat is always constant to reduce the output fluctuation of the system. The solar flux is not stable over the year, because of the special and temporal change of the incident solar intensity. Therefore, the use of cold and hot thermal storage for the HITEC fluid is essential for the stability of heat production to the combined system. The results of the solar farm are discussed later. The thermodynamic results of CCP are presented in Table S-1, which includes both the GC and RC subsystems. In addition, the mass fractions of air, fuel, gas, and R245fa are displayed for each state point and listed in Table S-2. The air enters GT cycle at 101.3 kPa, and is compressed to 1000 kPa, while the fuel exits from fuel tank at 4300 kPa and releases to the combustion chamber at 2000 kPa. The combustion pressure is at 1000 kPa, which is chosen for the turbine safety and limitation. The intermediate pressure is 350 kPa, which is calculated based on the square root of multiplied low and high pressures to obtain maximum efficiency at these conditions. The R245fa is circulating in the RC and pressurized from 700 to 4000 kPa. The minimum pressure is selected in the purpose of having saturated temperature of 75.62 °C (348.76 K), so that the condenser steam will be 72.7 °C at 35 kPa with a 150 kg/s, which will be used in the desalination system.

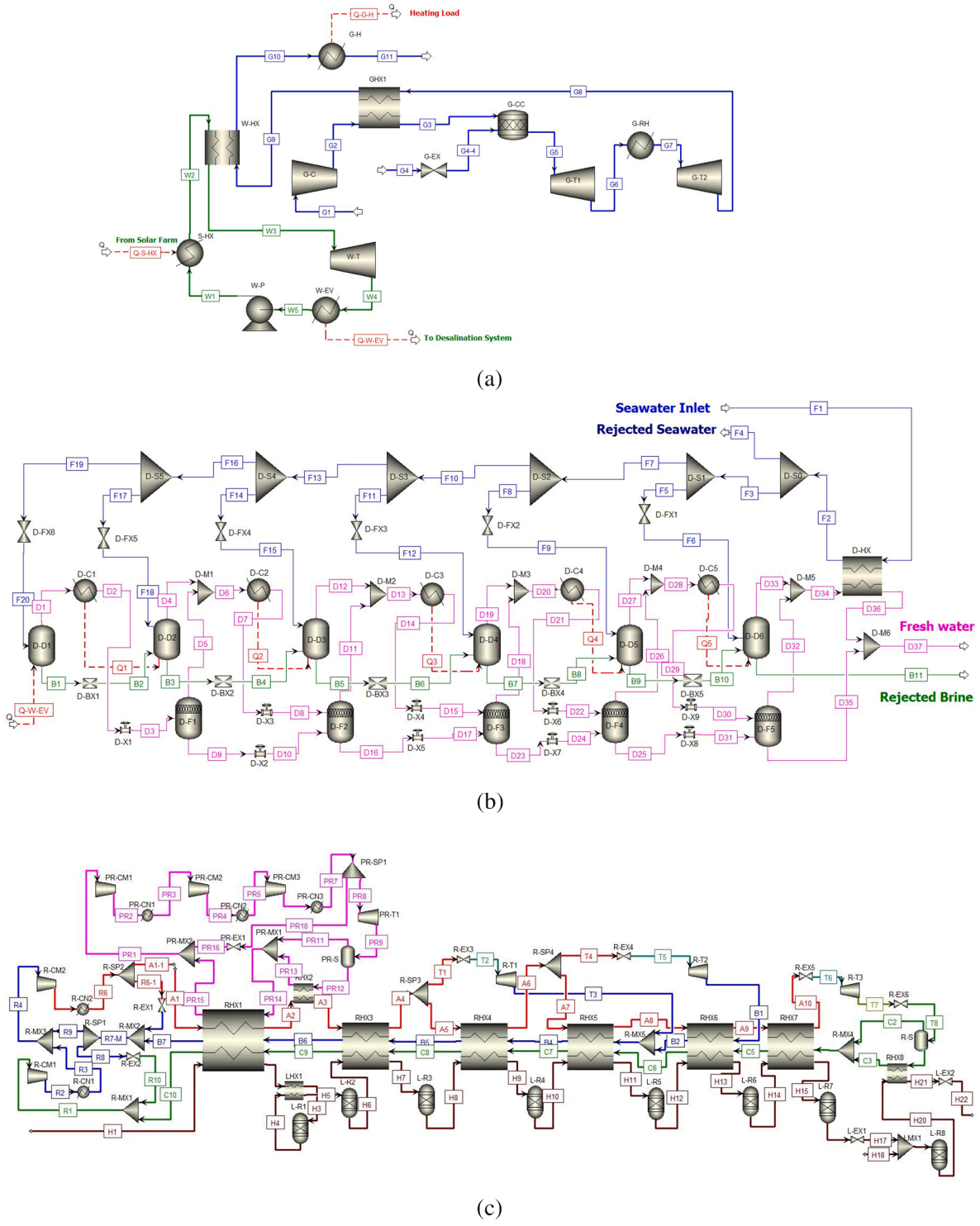

Fig. 3. The Aspen Plus flow charts for subsystems (a) the CCPP subsystem, (b) the MFD subsystem and (c) the hydrogen liquefaction system.

The energy of components is calculated as the heat and power from each component and the exergy destruction rate. Also, the energetic efficiency, exergetic efficiency, and the irreversibility ratio are evaluated for each component, as shown in Table S-3. The net power of the combined cycle is estimated to be 133.1 MW, while the heating load for residential buildings can be evaluated as 98.2 MW. The condenser heat rejection is calculated as 284 MW, which will be used for the desalination of seawater. The total exergy destruction of CCP is determined as 460.9 MW.

The multi-effects desalination systems have also been studied in this paper. The Aspen flowchart of MED system (Fig. 3-b) is different than displayed in the system layout (Fig. 1) because of new added processes for lowering and increasing pressures and mixing streams. The thermodynamic results of seawater streams are presented in Table S-4 and noted by F#. The seawater enters the stream are 900 kg/s, 10 °C, and 80 kPa. Then, it is heated to 52 °C (325.15 K) and distributed to the effects D-D1 to D-D6 at their operating pressures and cooled the distilled water by releasing the latent heat to be all in liquid phase. The total

Table 4
Thermodynamic settings and design assumptions for the integrated system.

Parameter					Remarks	
Ambient condition					298 K and 101.3 kPa	
LH_2 product					20 K, 130 kPa, 3.5155 kg/s (335 ton/day)	
Minimum temperature approach for heat exchangers					1–2.5 °C	
Equation of State					Peng-Robinson	
Adiabatic efficiency:						
Compressors					78–85% (worst case)	
Turbines					80–90% (state-of-the-art turbomachinery)	
Pumps					60% (worst case)	
Pressure drop in piping, connectors, mixers, splitters, heat exchangers, condensers, etc.					0 kPa (ideal case for this study)	
Cycles	SF	GC	Electro.	RC	MED	LH
Mass flow rate(s) [kg/s]	2000 to panels 1734 to S-HX	Air 390 Fuel 4.68	32.09	1270	F1 900 to D-HX F3 200 to Effects	N_2 44 H_2 7.5 LH_2 3.5515
Pressure levels [kPa]	200 500	101.3 350 1000	200	150 4000	101.3 98 96	N_2 100, 600, 3600, 20,000 H_2 200, 650, 2000 LH_2 200
Feed conditions	200 °C 200 kPa	12.2 °C 101.3 kPa	17 °C 200 kPa	50 °C 150 kPa	65 °C 101.3 kPa	17 °C 200 kPa

seawater mass flow rates are 740 kg/s and has a salinity of 35 kg/kg [42]. Table S-5 presents the thermodynamic results of distilled water (noted as D#). Since the seawater flow rate is distributed over the six effects, the distilled water is also distributed and ranges from 112.4 kg/s (D-D4) to 116.9 kg/s (D-D1) and temperature varies from 65.9 °C to 58.2℃ and has almost zero salinity. The cumulated distilled water is 684 kg/s at 14 kPa and 52.5 °C. The thermodynamic results of brine stream (noted as B#) are listed in Table S-6. The brine has a mass flow of the 23.14 kg/s and increases to 55.97 kg/s. the pressure of brine decreases 24 to 14 kPa, by step of 2 kPa. The brine temperature decreases from 65.9 °C to 58.2℃. The final brine (B11) and distilled water (D37) are in liquid phase.

The heat for MED components and their energetic and exergetic efficiencies are tabulated in Table S-7. The heat added to the first effect (D-D1) is estimated as 284 MW, which is from the combined system. The distilled steam from the effects provides heat to the seawater and separates the saline from the water, so the distilled steam cools to the liquid phase and flows to a flash box (noted as D-f# in Fig. 3-b) after it is expanded in the expansion valve to a lower pressure. The condensers (noted as D-C#) represents the released heat from the distilled steam to heat the following effect. As shown in Table S-7, the condenser loads vary from 277 to 271 MW with no energy loss and exergetic efficiency ranges from 75 to 97%. The total exergy destruction of desalination system is 190 MW. The exergy destructions of components are displayed in Fig. 4. The maximum exergy destruction is from effects (163.5 MW), while the minimum excluding the zero is form mixers (5.3 kW). The flash boxes and splitters have zero exergy destruction. This high exergy destruction is as a result of temperature difference to the standard

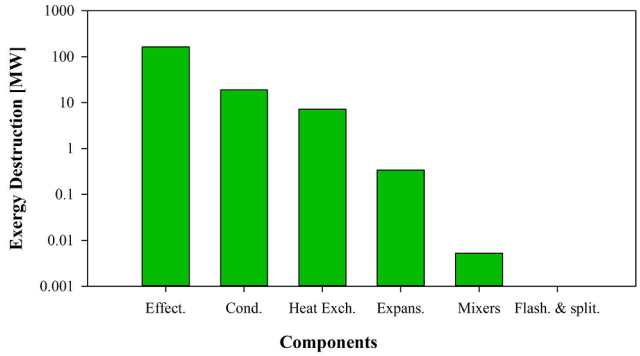

Fig. 4. The exergy destruction of components in the MED system.

conditions and the separation of brine from seawater. The amount of heat added to effects is displayed in Fig. 5-a. The effect pressure decreases while the heat decreases from D-D1 to D-D4, then increases for D-D5 and more for D-D6 because of the latent heat of steam transferred to the next effect. The mass flow rates of distilled water and brine are graphed in Fig. 5-b. The final results from the MED are 684.03 kg/s distilled water and 55.97 kg/s brine. The steam enters the D-D1 at 150 kg/s, 35 kPa, and 72.7 °C. Therefore, the GOR is 4.56 for six effects.

For the electrolyzer, the thermodynamic results and energy rates are displayed in Table S-8 and Table S-9, respectively. The amount of fresh water is 32.09 kg/s to produce hydrogen and oxygen gases of 3.566 and 28.52 kg/s, respectively. The electrolyzer power is calculated as 18.5 MW with a thermal efficiency of 60% and exergetic efficiency of 69%.

In addition, the thermodynamic results of the hydrogen liquefaction system are presented in Tables S-10 to S-12. The precooling refrigeration subsystem is operated using nitrogen gas, and the results of state points are listed in Table S-10. This precooling system circulates the nitrogen with 44 kg/s and pressurizes it from 100 kPa to 20 MPa in three levels (600 kPa, 3.6 MPa, and 20 MPa). The nitrogen starts its process at a temperature of 278.1 K and drops to 77.4 K. This system is valuable to the liquefaction since it removes more heat and helps to reduce the hydrogen from 290 K to 100 K in the heat exchanger RHX1.

In addition, the state point results of hydrogen Claude refrigeration system are presented in Table S-11. The hydrogen mass flow rate is 7.5 kg/s and is pressurized from 200 kPa to 650 kPa then to 2000 kPa. The lowest temperature is 30.4 K at 200 kPa. There are three paths of different pressure levels: A# for high pressure (2000 kPa) and mass flow rate varies from 6.75 to 5.47 kg/s, B# for intermediate pressure (650 kPa) with mass flow rates of 0.61 and 1.28 kg/s, and C# low pressure (200 kPa) with mass flow rates of 0.19, 5.28, 5.47 kg/s. Also, the results of liquefied hydrogen steam are given in Table S-12. The hydrogen flows with a rate of 3.5515 kg/s and cryogenically cooled from 290 K and 200 kPa to 20.01 K and 130 kPa.

The performance of the condensers is shown in Table 5 and Fig. 6-a. The maximum condenser heat was found in R-CN1 with about 27.7 MW and its exergy destruction rate is 762.4 kW, while the maximum exergy destruction rate was found in PR-CN2 of 1207 kW. The energetic and exergetic efficiencies are displayed in the same table. In addition, the specifications of reactors in the LH system are displayed in Table 6 and the exothermic heat of reactors is graphed in Fig. 6-b. The highest exothermic heat is for the first reactor L-R1to produce 0.5598 mass fraction of parahydrogen at 70 K, while the minimum exothermic heat is for L-R7 (4.9 kW) to produce 0.9922 mass fraction of parahydrogen.

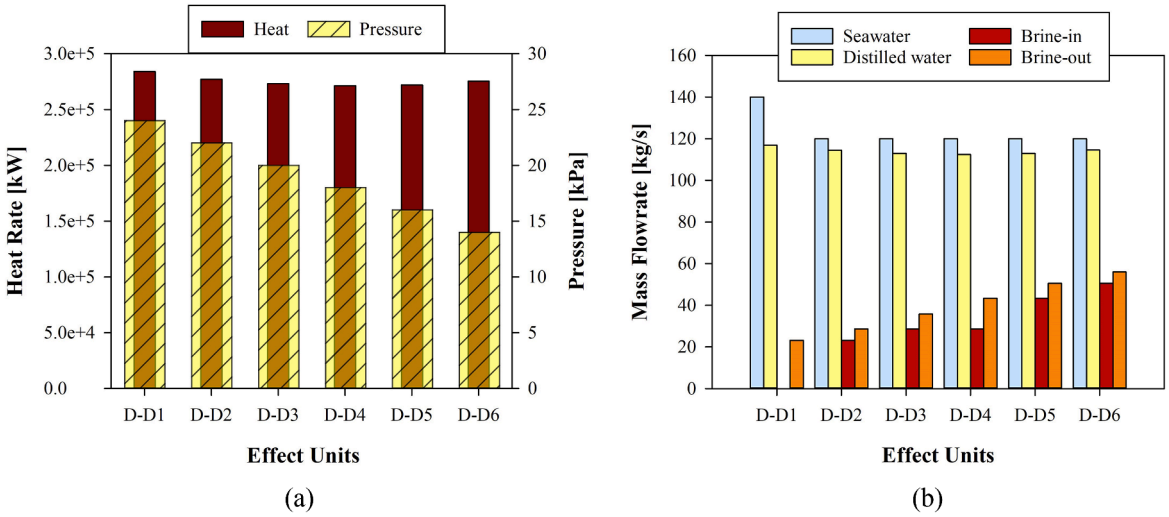

Fig. 5. The heat rate of effect units (a) and the mass flow rate of seawater, distilled water and brine for effect units (b).

Table 5
The energy performance of condensers in the LH system.

Items	$\dot{Q}$[kW]	$\dot{E}x_{des}$[kW]	η [%]	ψ [%]
PR-CN1	10409.9	943.1	100	16.43
PR-CN2	12001.0	1207.0	100	10.58
PR-CN3	15651.8	258.7	100	8.31
R-CN1	27673.2	762.4	100	29.33
R-CN2	14684.8	115.2	100	8.36

The duties and specifications of heat exchangers in the HL system are displayed in Table 7 and Fig. 7-a. The maximum duty is 30019.6 kW for the RHX1 to reduce the hydrogen temperature from 290 K to 100 K, while the minimum duty is 38.5 kW for the last heat exchanger RHX8 to reduce the temperature from 20.5 K to 20 K. Fig. 7-b shows the rejected heat through the heat exchangers with respect to the temperature of liquefied hydrogen. The amount of accumulated heat is estimated to be about 12,000 kW for the temperature range 100 K to 20 K, which is less than a half of the heat from 290 K to 100 K.

In addition, the performance of turbines are compressors are

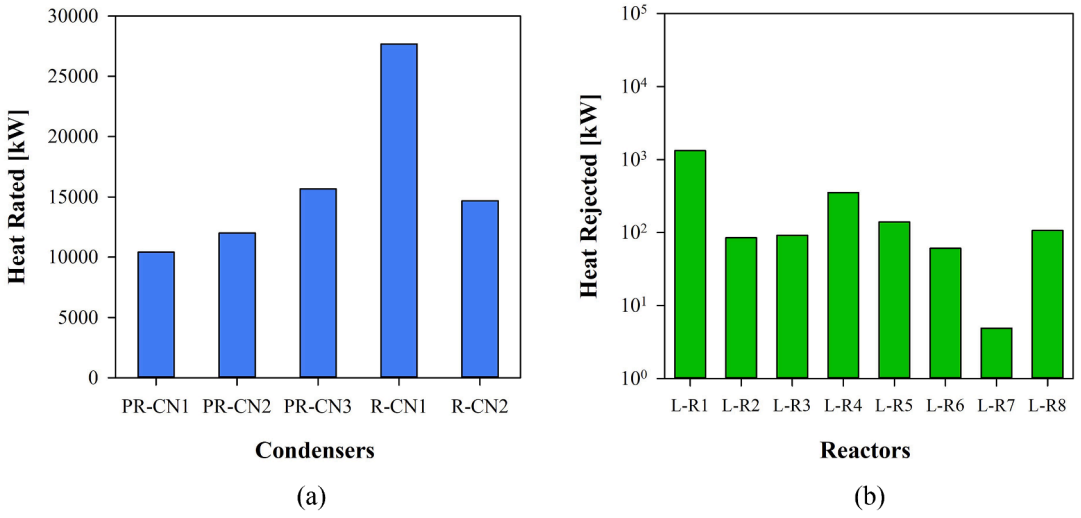

Fig. 6. The heat rate of condensers (a) and the exothermic heat of reactors (b).

Table 6
Specifications of reactors and their operating conditions, and total mass fraction of parahydrogen (Y_p).

Reactor	$\dot{Q}$ [kW]	$\dot{E}x_{des}$[kW]	η [%]	ψ [%]	T [K]	Y_p	C_0	C_1	C_2	K [%]
L-R1	1325.0	4657.7	77.62	24.26	70	0.5598	41.22	−1.57E−02	2.24E−04	41.3
L-R2	84.7	141.5	96.63	96.3	80	0.4855	31.398	−1.38E−02	1.72E−04	31.4
L-R3	91.2	400.6	98.07	91.69	68	0.5598	41.298	−1.62E−02	2.38E−04	41.3
L-R4	353.7	100.0	93.42	98.34	56	0.8290	77.198	−1.96E−02	3.51E−04	77.2
L-R5	139.2	357.1	97.46	70.07	44	0.9288	90.498	−2.50E−02	5.68E−04	90.5
L-R6	60.7	6848.1	98.93	54.02	32	0.9500	94.998	−3.67E−02	1.22E−03	95.0
L-R7	4.9	6869.2	99.87	50.63	22	0.9925	98.998	−5.00E−02	2.27E−03	99.0
L-R8	106.5	26604.1	98.39	9.61	20.5	0.9985	99.798	−5.37E−02	2.62E−03	99.8

Table 7
Specifications of heat exchangers in the LH syste.

Parameter	LHX1	RHX1	RHX2	RHX3	RHX4	RHX5	RHX6	RHX7	RHX8
LMTD [°C]	10.55	1.57	9.35	7.89	8.58	9.42	9.39	9.35	18.14
MTA [°C]	1.20	1.00	2.21	1.75	1.75	2.10	1.40	2.10	2.48
No. Paths	5	2	4	4	4	4	3	2	2
$\dot{Q}$[kW]	510.4	30019.6	466.2	917.6	995.0	992.2	1486.9	4038.9	34.5
$\dot{E}x_{des}$[kW]	331.2	1049.2	31.0	1027.3	1371.8	9949.4	6867.1	20220.9	1269.6
η [%]	100	100	100	100	100	100	100	100	100
ψ [%]	96.79	98.09	99.93	98.59	98.15	87.35	91.37	83.45	71.75

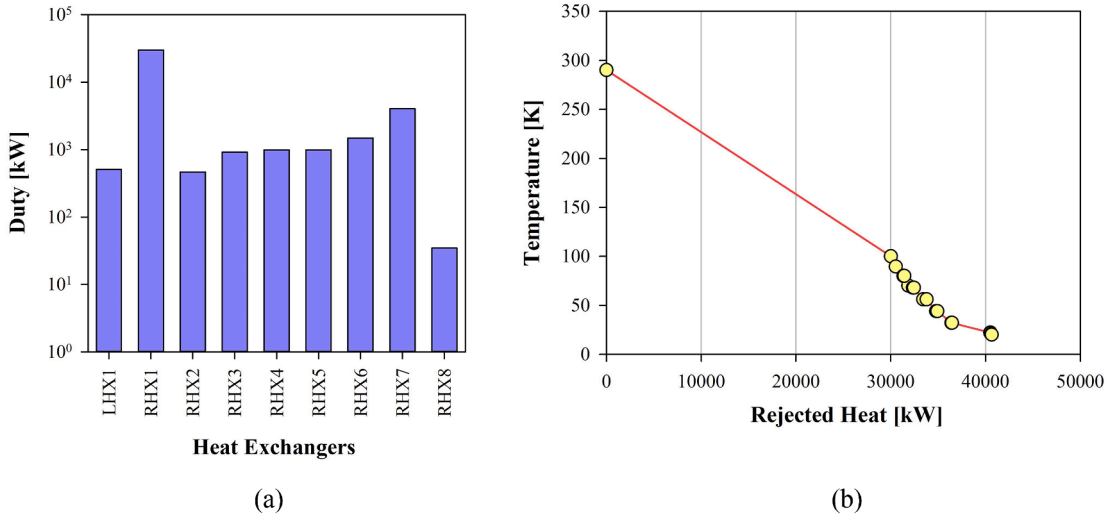

Fig. 7. The duty of heat exchangers (a) and the amount of rejected heat versus temperature of liquefied hydrogen (b).

Table 8
The performance of turbines and compressors in the LH system.

Items	$\dot{W}$ [kW]	$\dot{E}x_{des}$ [kW]	η [%]	ψ [%]
PR-CM1	10893.0	1497.9	78	86.25
PR-CM2	11400.3	1466.3	78	87.14
PR-CM3	10855.8	1449.5	78	86.65
PR-T1	4692.6	4521.1	80	53.67
R-CM1	27186.8	3240.4	80	88.08
R-CM2	15224.5	2155.3	80	85.84
R-T1	117.9	146.6	80	96.11
R-T2	99.1	130.6	80	99.73
R-T3	4284.8	8146.6	90	77.09

displayed in Table 8 and Fig. 8. The net power of the nitrogen cycle is 28.5 MW, while that of the hydrogen cycle is 37.9 MW. The maximum compressor power is 27.1 MW for R-CM1, while the maximum turbine power is 4.7 MW for PR-CM3.

The exergy destruction and the irreversibility rates (IR) from the components are displayed in Table S-13. The highest IR is 44.4% for the mixers, while the minimum IR is 1.4% for the condensers. The components with the highest exergy destruction are mixers, then reactors, then heat exchanger. Some components have zero exergy destruction, such as splitters and separators. The total exergy destruction is 235.3 MW.

5.2. Performance evaluation results

The performance of subsystems and the entire system are given in

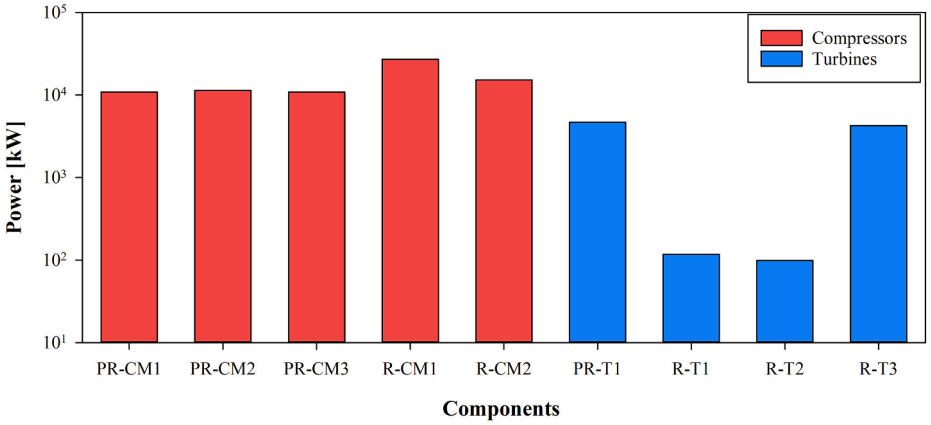

Fig. 8. The power of turbines and compressors of the HL system.

Table 9
The performance of subsystems and the integrated system.

Subsystem	Input Energy [kW]	Output Energy [kW]	η [%]	Input Exergy [kW]	Output Exergy [kW]	ψ [%]
Solar farm	451517.6	201320.0	44.59	420469.4	81333.3	19.34
Gas turbine	255577.1	199968.7	78.24	184816.2	126809.7	68.61
Rankine cycle	315419.6	315419.6	100.0	110205.5	73557.5	66.75
Combined cycle	707094.7	515388.3	72.9	605285.6	200367.2	33.11
Desalination	11834804.5	10638960.4	89.9	55668.3	14882.8	26.73
Electrolyzer	18493.6	13389.6	60.0	18493.6	14383.2	69.0
Precooling system	28456.5	9606.2	296.2	28456.5	9726.5	292.6
Refrigeration system	37909.6	14054.6	269.7	37909.6	18696.6	202.8
Hydrogen liquefaction	66366.1	16040.8	24.17	66366.1	51384.3	77.43
Entire system	12257833.2	10801468.2	88.12	605791.3	139575.1	23.05

Table 9. The solar farm has input energy as 451.6 MW coming from the incident solar radiation multiplied by the area of the unshaded collector aperture area of one module 69.4 m^2 and the number of modules (100) per collector and the number of loops (300). Since the incident solar radiation is low in Oshawa, the number of collectors should increase to maintain the constant heat source 201.3 MW of heat exchanger S-HX for CCP. Therefore, the solar farm has energetic and exergetic efficiencies of 44.59% and 19.34%, respectively.

The GC has input energy of 256 MW consisting of a combustion chamber and reheater to produce heating load and output energy of

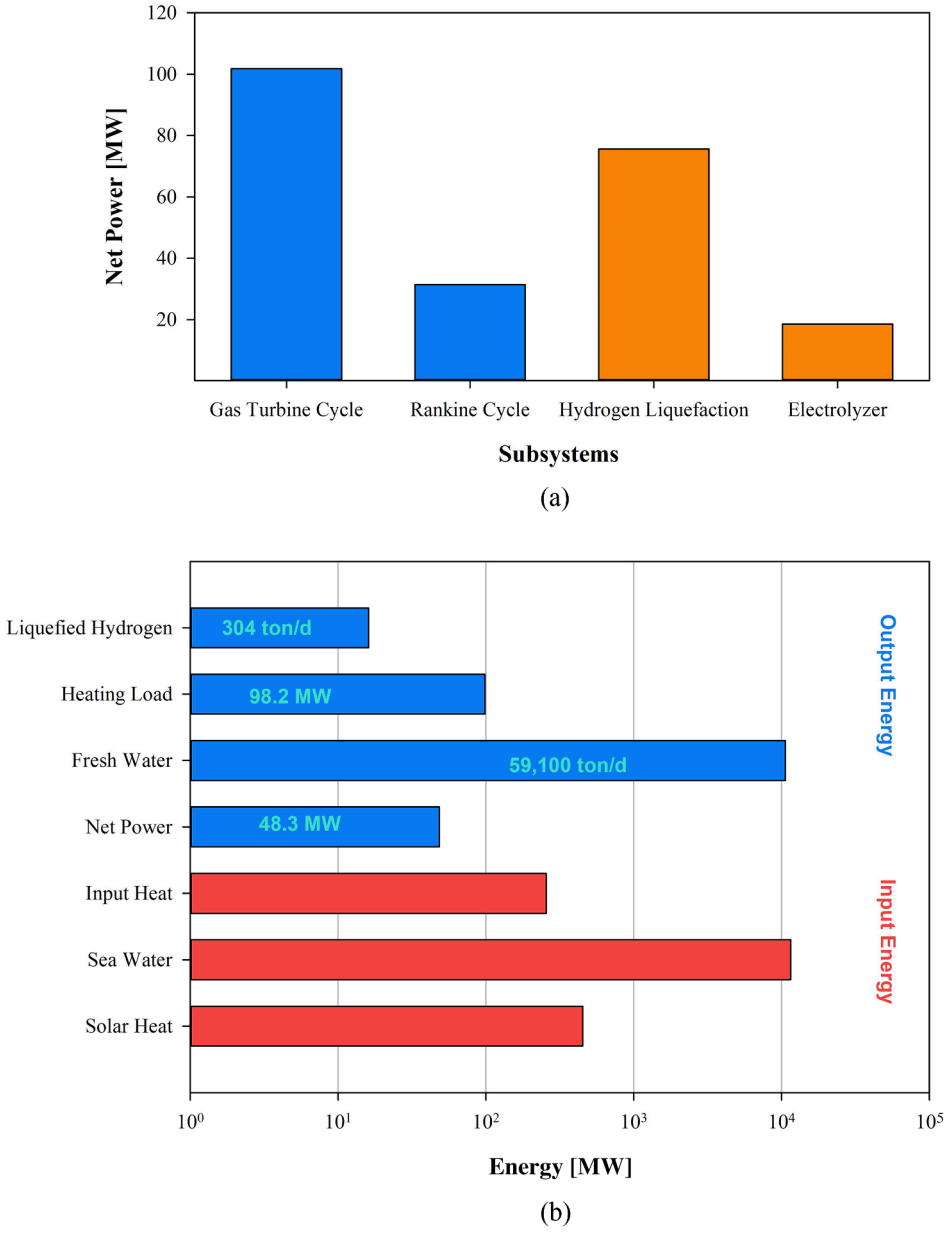

Fig. 9. The net power of subsystems (a) and the input and output energy rates for the integrated system (b).

201.3 MW, considering the net power of 107 MW, as shown in Fig. 9-a, and the heating loads 98.2 MW for residential buildings. The energetic and exergetic efficiencies are 78.24% and 68.61%, respectively.

The RC requires input energy of 315.4 MW, including the heating from the solar farm through the heat exchanger S-HX and the heating load from the GC heat exchanger W-HX. This cycle provides output energy of 315.4 MW consisting of the net power of 31.4 MW and the heating load of 284 MW for the desalination MED system. The energetic and exergetic efficiencies are 100% and 66.75%. Therefore, the combined cycle of the solar farm, GC, and RC can provide output energy of 707 MW and deliver an output energy of 515.4 MW. The input energy composes of incident solar radiation, combustion chamber, and reheater, while the output energy includes the heating load of 98.2 MW, the net power of 133.1 MW, and condenser heating load of 284 MW for the desalination system.

The desalination MED system has the input and output energy of 11.8 GW and 10.6 GW, which provides energetic and exergetic efficiencies of 89.9% and 26.73%, respectively. The GOR is 4.56. The input of seawater and the heating load is larger than the output energy of freshwater. The mass flow rate of seawater is 900 kg/s, 18% of it is used for cooling the freshwater while 82% of it is used for desalination. The total mass flow rate of fresh water is 684 kg/s, while the seawater flow rate is 740 kg/s are used for desalination. Some of the desalination water can be used in the electrolyzer to produce hydrogen and oxygen gases.

For the electrolyzer, the input energy is 18.5 MW, while the output energy is 13.4 MW for producing the hydrogen gas. Therefore, the energy and exergy efficiencies of electrolyzer are 60% and 69%, respectively.

The hydrogen liquefaction system consists of three subsystems. The precooling refrigeration has the net input power of 28.5 M, while it has an output cooling load of 9.6 MW through two heat exchangers RHX1 and RHX2. Therefore, the energetic and exergetic COP are 2.96 and 2.93, respectively. The second subsystem is the main hydrogen refrigeration system, which has input and output energy of 37.9 and 14.1 MW, respectively. The input and output energy are the net power and the cooling load of seven heat exchangers (RHX1, RHX3 to RHX8) to liquify the hydrogen. The energetic and exergetic COP of the main refrigeration subsystem is 2.7 and 2.03, respectively. The third subsystem is the liquefying stream. The whole liquefaction system has a total input energy of 66.4 MW and output energy od 16 MW. The energetic efficiency of the system is 24.17%, while the exergetic efficiency or FOM is 77.4%. The SCF of the liquefaction system is estimated to be 5.24 kWh/kg_{LH2}. The entire integrated system has input and output energy rates of 12.3 GW and 10.8 GW, respectively. That means the integrated system has the energetic and exergetic efficiencies of 88.12% and 23.05%, respectively.

The net power of each system is illustrated in Fig. 9-a. The net power of GC and RC is much greater than the electrolyzer, the HL, and the MED systems. Therefore, the gross power should be sufficient for the Kedron community, which needs about 8.3 MW. The gross power of the integrated plant is 48.3 MW.

The integrated system provides other useful outputs for the Kedron community, as shown in Fig. 9-b. The heating load is 98.2 MW, which is 60% more than the actual heating loads for the community because of future losses of piping connections. The amount of freshwater is 284 kg/s which is more than double the actual amount needed for the community. Part of this freshwater is used in electrolyzer, which is 32.09 kg/s. This increase is adequate to marketing and farming, which benefits the community in other aspects. The major input sources for the integrated system are solar intensity, seawater, and other heating sources used in the combustion chamber and reheater. The amount of seawater is much higher than other sources, almost 18%, which comes from 900 kg/s to remove the latent heat of the freshwater at the end desalination process, while the actual amount of seawater used in desalination is 740 kg/s. The exergy destruction rates of components in each system are displayed in Fig. 10. The major exergy destruction rates are from condensers and combustion chambers of combined cycles, effect units of MED, mixers of HL, and solar panels of the solar farm. These rates have five orders of magnitudes in kW. The main reasons for this increase are the chemical reactions and the temperature difference of the fluid compared to the

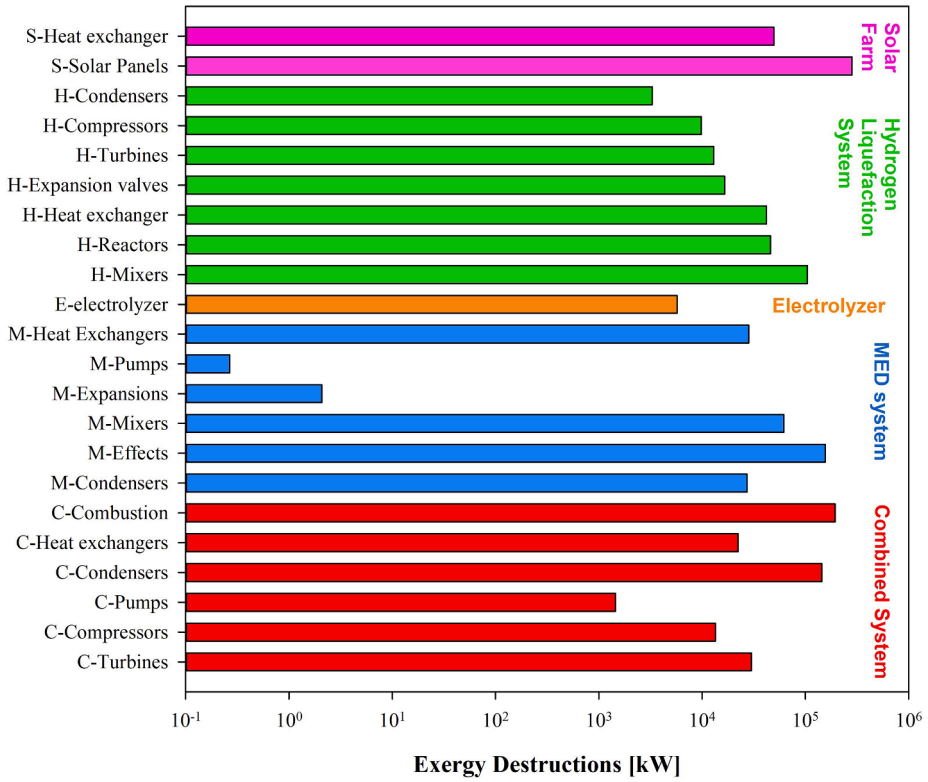

Fig. 10. The exergy destructions for components in each subsystem.

standard conditions (25 °C and 101.3 kPa).

5.3. Parametric studies

In this section, some parametric studies have been performed on the solar farm and CCP to investigate the effect of certain parameters on the system performance. The parametric studies are presented in the following subsections.

5.3.1. Solar radiation and solar farm output

In the city of Oshawa, the weather conditions are presented for four months, January, April, July, and October, as shown in Fig. 11. Theses weather conditions are air temperature in K, air velocity in m/s, and solar intensity in W/m^2. These months are chosen because the weather conditions in the city of Oshawa are more significant. The weather data were obtained from RETSCREEN software [43], which is a reliable software for weather data from Natural Resources Canada.

The change in weather conditions affects the solar flux of parabolic trough solar modules. Another parameter should be considered in establishing the solar units, which is the tilt angle of the panels, as shown in Fig. 12 (a). The tilt angle should be adjusted to gain maximum solar flux for each month, as shown in Fig. 12 (b). for the month of July, the maximum solar flux is 220 W/m^2, and the tilt angle is 16°, while for January, the solar flux is 180 W/m^{2,} and the tilt angle is 72°.

The heat rate through the collectors and the outlet flow temperature of HITEC fluid are presented in Fig. 13. Increasing the solar intensity will increase the heat rate and the outlet temperature as shown in the month of July compared to that of January. The inlet flow temperature is stable at 220 °C and must be above the melting temperature of HITEC which is 142 °C. The outlet flow ranges from 290 to 340 °C and must be lower than the maximum working temperature of 355 °C.

The energetic and exergetic efficiencies are graphed in Fig. 14 (a), which increases with decreasing the incident solar intensity and solar flux of parabolic trough panels. The thermal efficiency ranges from 56% to 42%, and the exergetic efficiency ranges from 25% to 19%. The reason for such an opposite relationship is explained in Fig. 14 (b). The output heat from the solar farm system is the heat transfer to the heat exchanger of S-HX to the combined cycles, which is constant over the year and equals to 201320 kW to maintain the output services all the year. Therefore, the heat transfer ratio of heat exchanger S-HX to the heat transfer rate of panels Qu decrease from 0.84 in January to 0.6 in July, while the ratio of heat transfer of panels to the solar flux is almost constant through the year fluctuating around 0.62.

5.3.2. Parametric study on CCP

The parametric studies are also performed on the CCP. The effect of mass flow rate of GC on the efficiencies and energy is presented in Fig. 15(a) and (b). Increasing the mass flow rate slightly declines the thermal efficiency but slowly increases the exergetic efficiency of the CCP. The left side of Fig. 15 shows the net power, the heat rate of the combustion chamber and the reheater for the GC. The net power of GC and RC jumped from 300 to 350 kg/s, then slightly declined to 390 kg/s then increased with a constant rate from 390 to 500 kg/s. The combustion heat significantly grows with the increase of mass flow rate. The reheater load moderately rises with the increase of mass flow rate. The different increasing rates for input energy sources of combustion and reheater loads compared to the useful output energy such as net power affects the efficiencies of the system.

Another parameter is the effect of the maximum pressure of the GC on the efficiencies and the energy rates. Since the GC has two turbines, the intermediate pressure is estimated as the optimal pressure as a square root of multiplied maximum and a minimum pressure of the cycle to provide maximum thermal efficiency for each change in the maximum pressure. Fig. 16 (a) shows the slightly decrease the thermal efficiency and the gradually decrease of the exergetic efficiency of CCP. To understand this behaviour, Fig. 16 (b) presents the variations of net power of RC and GC systems, the heat rates of combustion chamber and the reheater loads as input sources for the CCP. The net power steadily declines over the increase of maximum pressure. However, the input sources show two opposite trends: the slight increase of reheater load and the significant drop of the combustion heat. That means, at high pressure, the amount of combustion heat decreases because the high pressure increases the ignition of fuel and air mixture with less amount of heat needed. However, the high pressure increases the heating load of the reheater. The summation of different trends of input sources will slightly increase the input heating loads, which will lead to a slight decrease of thermal efficiency and hence the exergetic efficiency.

5.4. Economic assessment results

The economic assessment of the integrated power plant is performed based on the levelized cost of energy analysis taking the consideration the following assumptions: the discount rate is 12% the life of the plant is 30 years, no inflation rate is occurred during the life span, and the feed-in-tariff (FIT) is 0.01 $/kWh for exported electricity, there is no escalation rate for the electricity and fuel, and there is no governmental funds and loans. Table 10 presents the direct and indirect investment cost, yearly cash inflow, and yearly cash outflow. Also, Table 11 displays the economic analysis of the integrated power plant. According to the calculations, the total investment cost is $1.3 billions including direct costs such as installation field and trough collectors for solar farm, thermal storage, Brayton and Rankine cycles, heating system, desalination, electrolyzer and hydrogen liquefaction; and indirect costs such as fixed operating and maintenance costing, overheads, building, and

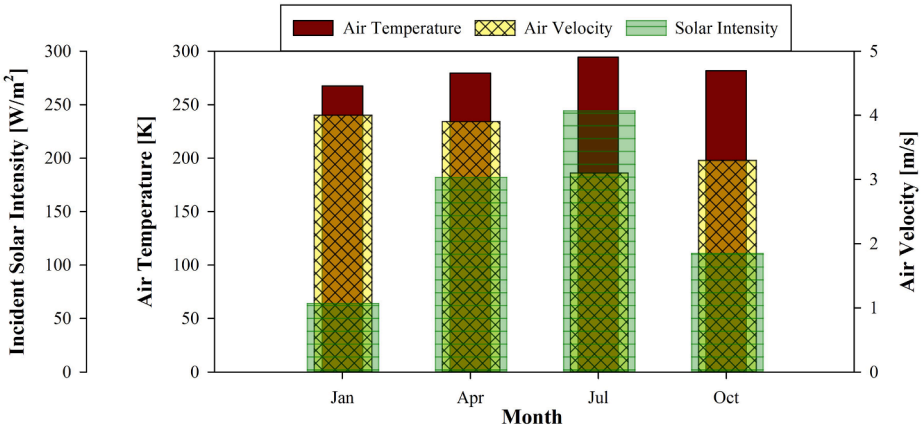

Fig. 11. The weather conditions of the city of Oshawa.

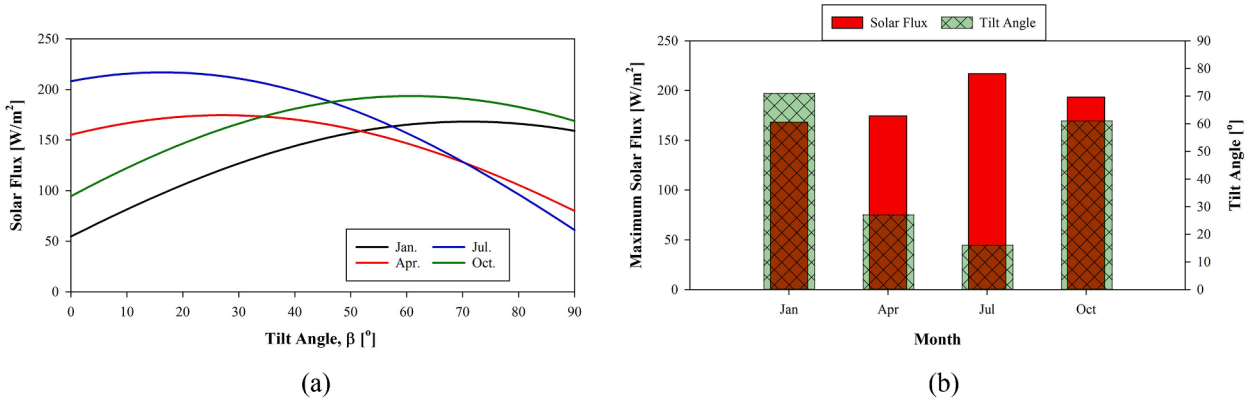

Fig. 12. The solar flux versus the tilt angle (a) and the maximum solar flux with respect to tilt angle in four months (b).

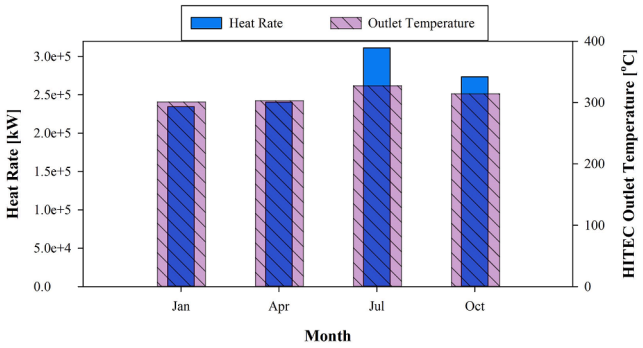

Fig. 13. The heat rate and the outlet temperature of HITEC of the solar panels.

land rental. The yearly cash outflow is about $79.8 millions to include variable operating and maintenance cost, production cost and fuel costs. Also, the yearly cash inflow is about $427.9 millions consisting of electricity generation cost, thermal heating, fresh water, liquefied hydrogen, and FIT costs.

The economic analysis shows that the integrated power plant is profitable since the profitability index is greater than 1 and the net present value is $1.5 billions. The discounted payback is 5.23 years as long as the discount rate, which is 12% is less than the interest rate of return (IRR) (26.74%). The levelized cost of energy is 14.59 $/MWh. Bakos and Parsa [44] investigated the concentration parabolic trough solar system economically and they found that the cost of energy is 0.04582 €/kWh which is equivalent to 54.43 $/MWh based on 1 € converts to 1.188 US$ [46].

Also, Rezaei et al. [47] studied the economic analysis of six power plants such as oil, gas, combined cycle, pressurized water reactor and pebble-bed modular reactor associated with MED desalination system. They found that the cost of energy ranges from 64.63$/MWh for the modular reactor to 161.32 $/MWh for fossil fuel. The cost of energy of the combined cycle is 97.72$/MWh. That means the current integrated power plant is economic due to many services in the yearly cash inflow costs.

5.5. Environmental impact assessment results

The exhaust gases from the plant is 394.68 kg/s which as the following mass fraction of 78.06% N_2, 16.11% O_2, 2.53% H_2O, and 3.30% CO_2. The environmental impact assessment for this system during the operation period is 46849.8 kg-CO_2eq. for GWP and 0 kg-O_3eq. for OZD. These emissions are equivalent to 0.35193 kg-CO_2eq/kWh$_{el}$ (0.098 kg-CO_2eq/MJ). The GWP for natural gas is 2, while for the R245fa is 1030. The GWP100 for HITEC is 2.914 kg-CO_2eq and ozone layer depletion is 2.75e-7 kg-CFC-11eq [48].

Klein and Rubin [49] studied the life cycle assessment of concen trated solar power (CSP) plant with three energy backup strategies such as minimal back up (MB), thermal energy storage (TES) with molten salt, and a natural gas-fired heater (NG) and dry and wet cooling systems. The life cycle assessment covers the global greenhouse emissions, onsite land use, and water consumption. They found that the natural gas combined cycle (NGCC) has emitted 400 kg-CO_2eq/MWh while combining with CSP reduced the GHG amounts to 90 kg-CO_2eq/MWh. The GHG emissions for CSP combined with TES, MD, and NG are 60–73, 35, and 127–317 kg-CO_2eq/MWh. The TES-CSP has larger onsite land footprint than others and similar water consumption. In addition, Piemonte et al. [50] performed a life cycle analysis on existing CSP such as MS-CSP in Italy to produce 1.58 MW$_{th}$. The GWP100a was obtained to be 0.190 kg-

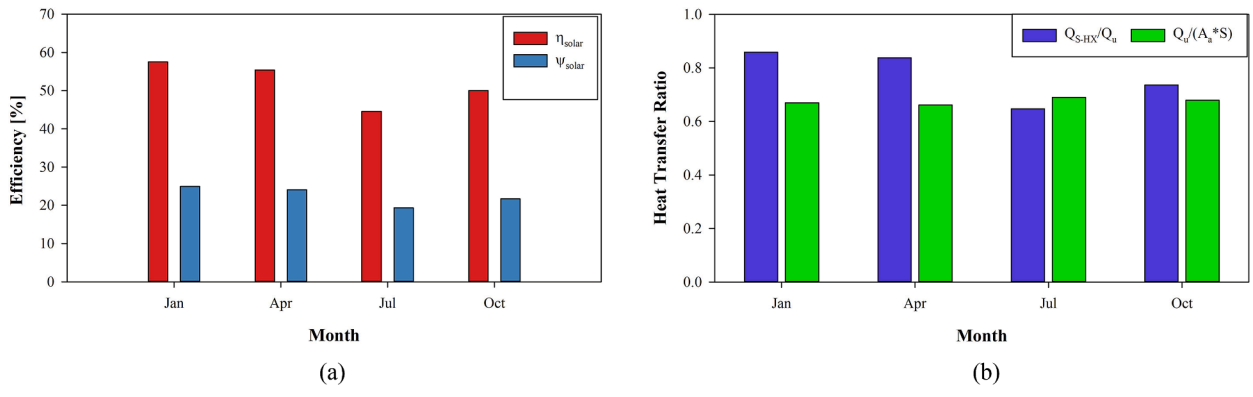

Fig. 14. The energetic and exergetic efficiencies of solar farm (a) and the heat transfer ratios (b).

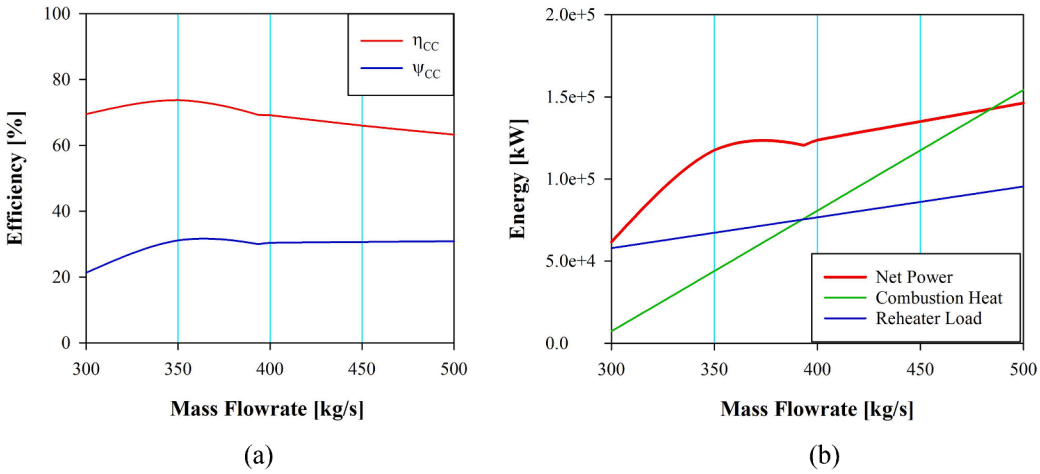

Fig. 15. The effect of air mass flow rate to efficiencies (a) and energy rates (b).

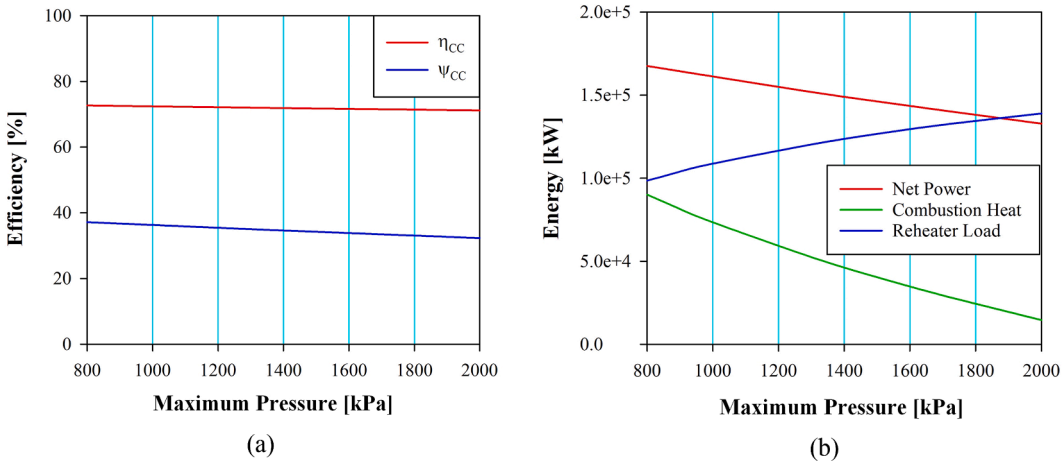

Fig. 16. The effect of maximum pressure on the efficiencies (a) and the energy rates (b).

CO_2eq/kWh_{el}, which was less than natural gas power plant (0.934 kg-CO_2eq/kWh_{el}). Also, the CSP has less OZP (1.26E-08 kg-CFC-11eq) than that of natural gas but higher cumulative energy demand (24.45 MJeq) compared to that of natural gas (0.033 MJeq).

For molten salts, Batuecas et al. [48] performed a life cycle analysis on different heat transfer fluids that used in parabolic trough concentrated solar power plant. They studied Therminol (a thermal oil), binary salt mixture composed of 40% KNO_3 and 60% of $NANO_3$, and ternary solar salt mixture HITEC. The life cycle assessment should that the HITEC molten salt have the lowest values in abiotic depletion, global warming potential, human toxicity, photochemical oxidation, acidification, and eutrophication potential categories compared to others. However, it has higher values of ozone layer depletion and terrestrial ecotoxicity than that of binary salt and lower than that of Therminol. After applying the normalization factor according to EU25 database, HITEC has the least environmental impact compared to binary salt and Therminol.

For the selected refrigerant, Ameri and Jorjani [51] investigated the environmental impact and energy performance of three refrigerants such as R134a, R245fa, and R123. R245fa has minimum global warming and ozone depletion potential values than that of R123 and R134a. In addition, the R245fa produces an electric power of 184.6 kW for (ORC) and 1563 m^3/day fresh water in desalination system. The R123 contributes to higher electric power and less desalination production and R134a produces less electric power and less desalinated water.

5.6. Uncertainties and limitations

Some uncertainty factors may slightly affect the present calculations. These factors can be classified into four groups. First, the uncertainty of environmental conditions includes the air temperature, relative humidity, and solar index. Since the current simulations count on the RETscreen data presenting the monthly average weather conditions, which might not represent the actual weather conditions in the city of Oshawa. Second, the parabolic trough calculations depend on the environmental conditions especially the air temperature and the incident solar intensity. Therefore, the uncertainty of environmental conditions slightly affect the thermal energy by 4.7% and thermal efficiency by 3.9% [52]. Third, the uncertainty of pressure, temperature, and mass flowrate are not considered since the main simulation assumptions are constant inflow conditions through the system because they have slight effect on the power and heat transfer by an average of 3.9% and energetic and exergetic efficiencies by 3.45% [52]. Fourth, the uncertainty of capital cost and fuel prices have a significant impact on the levelized cost of energy and payback period [47] due to market instability through the world. The limitations of the current study is not using daily environmental data and pressure loss through the system, which might have slight effect on the overall thermal and exergetic performance.

Table 10
The investment, cash inflow and cash outflow costs of the integrated power plant [44,45].

Cost	Unit	value	Annual cost $/yr
Direct Costs			
Installation field preparation	$/m^2	17.74872	$ 97,617,960.00
Trough collectors	$/m^2	260	$ 572,000,000.00
Thermal storage cost	$/kWh$_{th}$	13.2	$ 26,574,240.00
Brayton cycle	$/kW	301.97772	$ 30,731,877.58
Rankine cycle	$/kW	1011.3444	$ 31,709,058.77
Heating system	$/kWh	0.5 (heating season)	$ 156,776,300.00
Desalination	$/m^3/day	1695	$ 103,732,233.37
Electrolyzer	$/kWh	0.15	$ 24,300,569.95
Hydrogen liquefaction	$/kW	1299	$ 86,209,519.74
Subtotal-1			$ 1,129,651,759.40
Indirect Costs			
Fixed O&M	%	5	$ 56,482,587.97
Overheads (contingency)	%	10	$ 112,965,175.94
Building	%	0.1	$ 1,129,651.76
Land rental	%	0.05	$ 564,825.88
Subtotal-2	$		$ 171,142,241.55
Initial cost of investment	$		$ 1,300,794,000.95
Yearly cash outflow			
Variable O&M cost	$/MWh	10	$ 4,227,787.56
Production cost	$/kWh	0.003	$ 1,268,336.27
Fuel costs			
HITEC cost per kg	$/kg	0.93	$ 1,334,735.23
Fuel mixture	$/GJ	0.08	$ 624,594.45
Nitrogen	$/m^3	0.03	$ 4,027.12
Hydrogen	$/kg-$H_2$	0.216	$ 5,832.00
R245fa	$/kg	5	$ 21,600,000.00
Emissions	$/tonne	20	$ 50,668,790.66
Total cash outflow	$		$ 79,734,103.30
Yearly cash inflow			
Electricity	$/kWh	0.1	$ 42,277,875.65
Heating	$/kWh$_{th}$	0.25	$ 78,388,150.00
Fresh water	$/lit	0.01	$ 215,714,967.32
LH	$/kg-$LH_2$	0.7866	$ 87,208,738.59
FIT electricity	$/kWh	0.01	$ 4,227,787.56
Total cash inflow	$		$ 427,817,519.13

Table 11
The economic analysis of integrated power plant.

Item	Value
Net present value (NPV)	$ 1,503,081,949.70
Interest rate of return (IRR)	26.74%
Discounted payback (DPB)	5.23 years
Profitability index (PI)	2.16
Return of investment (ROI)	77.36%
Levelized cost of energy (LCOE)	14.59 $/MWh

6. Conclusions

This paper presents a novel integrated large-scale combined cycle power plant (CCPP). It combines several subsystems to provide several services for the Kedron Community in the city of Oshawa in Canada. This system depends on renewable sources such as solar radiation and seawater from the Atlantic Ocean to provide clean and sustainable energy. The CCPP consists of several subsystems: a solar farm, a gas turbine cycle, a Rankine cycle, a desalination MED, an electrolyzer, and a hydrogen liquefaction subsystem. The main conclusions are the following:

- The solar farm has 30,000 panels to absorb solar radiation and produce a constant heat of 201.3 MW for the combined cycle. The flowing fluid is HITEC with a total of 2000 kg/s through the parabolic troughs. The thermal and exergetic efficiencies are about 45% and 19%, respectively.
- The combined cycle consists of GC and RC that provide electric power, heating load for residential buildings, and heating load for the desalination systems. The services are 133.1 MW electric power, 98.2 MW residential heating loads, and 284 MW heating load for desalination. The thermal and exergetic efficiencies are about 73% and 33%, respectively.
- The desalination MED system uses 284 MW to provide a 684 kg/s freshwater from 740 kg/s seawater. Also, this system uses a 900 kg/s of seawater to remove the latent heat of freshwater to keep the liquid phase. The thermal and exergetic efficiencies are 89.9% and 26.73%, respectively.
- A water electrolyzer is used to produce 3.566 kg/s of hydrogen gas from the freshwater at a mass flow rate of 32.05 kg/s. The required power is estimated to be 18.5 MW. The thermal and exergetic efficiencies of the electrolyzer are 60% and 69%, respectively.
- The hydrogen liquefaction system consists of the hydrogen Claude refrigeration system and nitrogen precooling system to produce 335 ton/day of liquefied hydrogen. The mass flow rates of hydrogen and nitrogen in the refrigeration systems are 7.5 kg/s and 44 kg/s, respectively. The liquefaction power consumption is determined to be 66.4 MW with a specific energy consumption of 5.24 kWh/kg$_{LH2}$. The energy and exergy efficiency of the process is found to be about 24% and 77%, respectively.
- The gross output services are 48.3 MW electric power, 684 kg/s of freshwater, 355 ton of liquified hydrogen for clean fueling, 98.4 MW of heating load for residential buildings, which are more than the Kedron community needs. That means the gross output services can be fourfold the community's services.
- Parametric studies are performed to improve the system performance. The solar flux of solar PT is affected by the tilt angle and solar intensity. To gain maximum solar flux, the tilt angle must be 72° in January and 16° in July. The thermal efficiency ranges from 56% to 44%, while the exergy efficiency varies from 25% to 19% over the year. In addition, the change in the mass flow rate of air and the maximum pressure of GC are studied. Increasing the mass flow rate of air increases the net electric power and the input heat loads of combustion and reheater. Also, increasing the maximum pressure increases only the reheater load and decreases the net power and combustion heat. Therefore, increasing the maximum pressure slightly affects the efficiencies, while the increased mass flow rate increases the efficiencies.
- The integrated power plant has the cost of energy to be 14.59 $/MWh, which is economic due to multiple services that are provided to the community. Also, the amount of emissions is significantly low which makes this power plant environmentally benign.

Finally, the innovative integrated system presented here provides clean services for the Kedron community, but could be applied to other communities. The CCPP is considered an ecofriendly approach to produce electric power, heating load, freshwater, and liquefied hydrogen fueling for enhancing environmental sustainability.

Further analyses will be performed in near future focusing on multi-objective optimization, exergoenvironmental, and exergoeconomic analysis for a more comprehensive assessment of the proposed system for practical applications.

CRediT authorship contribution statement

Shaimaa Seyam: Methodology, Software, Writing - original draft, Investigation, Visualization. **Ibrahim Dincer:** Supervision, Conceptualization, Funding acquisition. **Martin Agelin-Chaab:**

Conceptualization, Funding acquisition.

Declaration of Competing Interest

The authors declare that they have no known competing financial interests or personal relationships that could have appeared to influence the work reported in this paper.

Acknowledgement

This research is supported by the Natural Sciences and Engineering Research Council of Canada (NSERC).

Appendix A. Supplementary data

Supplementary data to this article can be found online at https://doi.org/10.1016/j.enconman.2020.113434.

References

[1] Natural Resources Canada. About Electricity | Natural Resources Canada n.d. https://www.nrcan.gc.ca/energy/electricity-infrastructure/about-electricity/7359 (accessed June 9, 2020).
[2] Electricity facts | Natural Resources Canada n.d. https://www.nrcan.gc.ca/science-data/data-analysis/energy-data-analysis/electricity-facts/20068 (accessed June 16, 2020).
[3] Energy Facts | Natural Resources Canada n.d. https://www.nrcan.gc.ca/science-data/data-analysis/energy-data-analysis/energy-facts/20061 (accessed November 29, 2019).
[4] Ceylan Z. Investigation the insights between health expenditures and air quality. Int J Glob Warm 2020;20:203–15. https://doi.org/10.1504/IJGW.2020.106594.
[5] Saxena G, Gaur MK. Exergy analysis of evacuated tube solar collectors. A review. Int J Exergy 2018;25:54–74. https://doi.org/10.1504/IJEX.2018.088887.
[6] Askari IB, Ameri M. Solar rankine cycle (SRC) powered by Linear Fresnel solar field and integrated with Multi Effect Desalination (MED) system. Renew Energy 2018;117:52–70. https://doi.org/10.1016/j.renene.2017.10.033.
[7] Mehrpooya M, Tosang E, Dadak A. Investigation of a combined cycle power plant coupled with a parabolic trough solar field and high temperature energy storage system. Energy Convers Manag 2018;171:1662–74. https://doi.org/10.1016/j.enconman.2018.07.001.
[8] Frantz C, Seifert B. Thermal analysis of a multi-effect distillation plant powered by a solar tower plant. Energy Procedia 2015;69:1928–37. https://doi.org/10.1016/j.egypro.2015.03.190.
[9] Berstad DO, Stang JH, Neksa P. Large-scale hydrogen liquefier utilising mixed-refrigerant. Int J Hydrogen Energy 2010;35:4512–23. https://doi.org/10.1016/j.ijhydene.2010.02.001.
[10] Aasadnia M, Mehrpooya M. Conceptual design and analysis of a novel process for hydrogen liquefaction assisted by absorption precooling system. J Clean Prod 2018;205:565–88. https://doi.org/10.1016/j.jclepro.2018.09.001.
[11] Seyam S, Al-hamed KHM, Qureshy AMMI, Dincer I. Multi-objective optimization of hydrogen production in hybrid renewable energy systems. Wellington, New Zealand: IEEE Congr. Evol. Comput.; 2019. p. 850–7.
[12] Seyam S, Dincer I, Agelin-Chaab M. A clean hydrogen liquefaction plant integrated with a geothermal system. J Clean Prod 2019;243:118562. https://doi.org/10.1016/j.jclepro.2019.118562.
[13] Murugan A. Iron-containing perovskite materials for stable hydrogen production by chemical looping water splitting. Newcastle University; 2011.
[14] White JF. Development of High-Activity Para- to Ortho-Hydrogen Conversion Catalysts. Volume 2. vol. 2. 2016.
[15] Service Oshawa. City of Oshawa: Community Profile 2017. Oshawa Bus Invest 2017. www.oshawa.ca/business-and-investment/resources/2017_Community_Profile_Complete-2.pdf (accessed February 13, 2020).
[16] Development Services Department. Oshawa: Development Services Committee. Oshawa Agendas 2013. http://app.oshawa.ca/agendas/development_services/2013/05-06/DS-13-137.pdf (accessed February 13, 2020).
[17] Statistics Canada. The Daily — Survey of Drinking Water Plants, 2017. Goverment of Canada 2019. https://www150.statcan.gc.ca/n1/daily-quotidien/190611/dq190611b-eng.htm (accessed February 13, 2020).
[18] Household energy consumption, Canada and provinces n.d. https://www150.statcan.gc.ca/t1/tbl1/en/tv.action?pid=2510006001 (accessed February 13, 2020).
[19] BC-Hydro. The average power usage for a residential customer . BC Hydro 2020. https://www.bchydro.com/search.html?q=What+is+the+average+power+usage+for+a+residential+customer%3F&qid=1429&ir_type=3 (accessed February 18, 2020).
[20] Wilson L. Average household electricity use around the world. Shrink That Footpr n.d. http://shrinkthatfootprint.com/average-household-electricity-consumption (accessed February 18, 2020).
[21] Seyam S, Dincer I, Agelin-Chaab M. Thermodynamic analysis of a hybrid energy system using geothermal and solar energy sources with thermal storage in a residential building. Energy Storage 2019. https://doi.org/10.1002/est2.103.
[22] Dias Pereira L, Raimondo D, Corgnati SP, Gameiro Da Silva M. Energy consumption in schools – A review paper. Renew Sustain Energy Rev 2014;40:911–22. https://doi.org/10.1016/j.rser.2014.08.010.
[23] Kim TW, Kang BJ, Kim H, Park CW, Hong WH. The study on the Energy Consumption of middle school facilities in Daegu, Korea. Energy Rep 2019;5:993–1000. https://doi.org/10.1016/j.egyr.2019.07.015.
[24] Kedron - Google Maps n.d. https://www.google.com/maps/place/Kedron,+Oshawa,+ON/@43.9653947,-78.8574767,4204m/data=!3m1!1e3!4m5!3m4!1s0x89d51b1efb581b75:0xa654fa1eff67dc40!8m2!3d43.953098!4d-78.882507 (accessed February 13, 2020).
[25] Leachman JW, Jacobsen RT, Penoncello SG, Lemmon EW. Fundamental equations of state for parahydrogen, normal hydrogen, and orthohydrogen. J Phys Chem Ref Data 2009;38:721–48. https://doi.org/10.1063/1.3160306.
[26] Noh J, Fulgueras AM, Sebastian LJ, Lee HG, Kim DS, Cho J. Estimation of thermodynamic properties of hydrogen isotopes and modeling of hydrogen isotope systems using Aspen Plus simulator. J Ind Eng Chem 2017;46:1–8. https://doi.org/10.1016/j.jiec.2016.07.053.
[27] Peng DY, Robinson DB. A new two-constant equation of state. Ind Eng Chem Fundam 1976;15:59–64. https://doi.org/10.1021/i160057a011.
[28] Goldmann G, Tödheide K. Equation of state and thermodynamic properties of molten potassium chloride to 1320 K and 6 Kbar. Zeitschrift Fur Naturforsch - Sect A J Phys Sci 1976;31:769–76. https://doi.org/10.1515/zna-1976-0715.
[29] Xu T, Karsten P. Thermophysical properties of sodium nitrate and sodium chloride solutions and their effects on fluid flow in unsaturated media. No. LBNL-48913. Berkeley, CA (United States): Lawrence Berkeley National Lab. (LBNL); 2001.
[30] Boerema N, Morrison G, Taylor R, Rosengarten G. Liquid sodium versus Hitec as a heat transfer fluid in solar thermal central receiver systems. Sol Energy 2012;86:2293–305. https://doi.org/10.1016/j.solener.2012.05.001.
[31] Geyer M, Lüpfert E, Osuna R, Esteban A, Schiel W, Schweitzer A, et al. EUROTROUGH-Parabolic Trough Collector Developed for Cost Efficient Solar Power Generation. n.d.
[32] Burkholder F, Kutscher C. Heat-Loss Testing of Solel's UVAC3 Parabolic Trough Receiver. 2008.
[33] Hydrocarbon Chromatographic Standards. Air Liq Am Spec Gases LLC 2020. www.ALspecialtygases.com (accessed February 24, 2020).
[34] Honeywell. Safety data sheet. HFC-245fa, Genetron ® 245fa. 2019.
[35] Dincer I, Acar C. Review and evaluation of hydrogen production methods for better sustainability. Int J Hydrogen Energy 2014;40:11094–111. https://doi.org/10.1016/j.ijhydene.2014.12.035.
[36] Carmo M, Fritz DL, Mergel J, Stolten D. A comprehensive review on PEM water electrolysis. Int J Hydrogen Energy 2013;38:4901–34. https://doi.org/10.1016/j.ijhydene.2013.01.151.
[37] McCarty RD, Hord J, Roder HM. Selected Properties of Hydrogen. 1981.
[38] Wilhelmsen Ø, Berstad D, Aasen A, Nekså P, Skaugen G. Reducing the exergy destruction in the cryogenic heat exchangers of hydrogen liquefaction processes. Int J Hydrogen Energy 2018;43:5033–47. https://doi.org/10.1016/j.ijhydene.2018.01.094.
[39] Sullivan NS. Ortho – para hydrogen at low temperature. Encycl. Magn. Reson. John Wiley & Sons, Ltd; 2007. doi:10.1002/9780470034590.emrstm0366.
[40] Asadnia M, Mehrpooya M. A novel hydrogen liquefaction process configuration with combined mixed refrigerant systems. Int J Hydrogen Energy 2017;42:15564–85. https://doi.org/10.1016/j.ijhydene.2017.04.260.
[41] Mehrpooya M, Sadaghiani MS, Hedayat N. A novel integrated hydrogen and natural gas liquefaction process using two multistage mixed refrigerant refrigeration systems. Int J Energy Res 2020;44:1636–53. https://doi.org/10.1002/er.4978.
[42] Sharqawy MH, Lienhard VJH, Zubair SM. Thermophysical properties of seawater. A review of existing correlations and data. Desalin Water Treat 2010;16:354–80. https://doi.org/10.5004/dwt.2010.1079.
[43] RETScreen | Natural Resources Canada n.d. https://www.nrcan.gc.ca/energy/retscreen/7465 (accessed September 25, 2019).
[44] Bakos GC, Parsa D. Technoeconomic assessment of an integrated solar combined cycle power plant in Greece using line-focus parabolic trough collectors. Renew Energy 2013;60:598–603. https://doi.org/10.1016/j.renene.2013.05.025.
[45] Kumar R, Sharma AK, Tewari PC. Cost analysis of a coal-fired power plant using the NPV method. J Ind Eng Int 2015;11:495–504. https://doi.org/10.1007/s40092-015-0116-8.
[46] Euro to US-Dollar Conversion | EUR to USD Exchange Rate Calculator | Markets Insider n.d. https://markets.businessinsider.com/currency-converter/euro_united-states-dollar (accessed August 13, 2020).
[47] Rezaei A, Naserbeagi A, Alahyarizadeh G, Aghaei M. Economic evaluation of Qeshm island MED-desalination plant coupling with different energy sources including fossils and nuclear power plants. Desalination 2017;422:101–12. https://doi.org/10.1016/j.desal.2017.08.016.
[48] Batuecas E, Mayo C, Díaz R, Pérez FJ. Life Cycle Assessment of heat transfer fluids in parabolic trough concentrating solar power technology. Sol Energy Mater Sol Cells 2017;171:91–7. https://doi.org/10.1016/j.solmat.2017.06.032.
[49] Klein SJW, Rubin ES. Life cycle assessment of greenhouse gas emissions, water and land use for concentrated solar power plants with different energy backup systems. Energy Policy 2013;63:935–50. https://doi.org/10.1016/j.enpol.2013.08.057.

[50] Piemonte V, De Falco M, Tarquini P, Giaconia A. Life Cycle Assessment of a high temperature molten salt concentrated solar power plant. Sol Energy 2011;85: 1101–8. https://doi.org/10.1016/j.solener.2011.03.002.

[51] Ameri M, Jorjani M. Performance assessment and multi-objective optimization of an integrated organic Rankine cycle and multi-effect desalination system. Desalination 2016;392:34–45. https://doi.org/10.1016/j.desal.2016.04.009.

[52] Kearney D. Utility-Scale Parabolic Trough Solar Systems. Performance Acceptance Test Guidelines. April 2009 - December 2010. Nrel 2011.